Journal of Medicinal Chemistry

Article

Identification of Highly Selective Lipoprotein-Associated Phospholipase A2 (Lp-PLA2) Inhibitors by a Covalent-Fragment-Based Approach

Fubao Huang, Hangchen Hu, Kai Wang, Chengyuan Peng, Wenwei Xu, Yu Zhang, Jing Gao, Yishen Liu, Hu Zhou, Ruimin Huang, Minjun Li, Jianhua Shen, and Yechun Xu

J. Med. Chem., **Just Accepted Manuscript** • DOI: 10.1021/acs.jmedchem.0c00372 • Publication Date (Web): 27 May 2020

is published by the American Chemical Society. 1155 Sixteenth Street N.W., Washington, DC 20036

Identification of Highly Selective Lipoprotein-Associated Phospholipase A2 (Lp-PLA2) Inhibitors by a Covalent-Fragment-Based Approach

Fubao Huang[a,#], Hangchen Hu[a,b,#], Kai Wang[a], Chengyuan Peng[a], Wenwei Xu[a], Yu Zhang[a], Jing Gao[b], Yishen Liu[c], Hu Zhou[a], Ruimin Huang[a], Minjun Li[d], Jianhua Shen[a] and Yechun Xu[a,b]**

[a]State Key Laboratory of Drug Research, CAS Key Laboratory of Receptor Research, Shanghai Institute of Materia Medica, Chinese Academy of Sciences, Shanghai 201203, China.

[b]University of Chinese Academy of Sciences, Beijing 100049, China.

[c]Nanchang University, Nanchang 330031, China.

[d]Shanghai Synchrotron Radiation Facility, Shanghai Advanced Research Institute,

Chinese Academy of Science, Shanghai 201203, China

ABSTRACT

Covalent ligands are of great interest as therapeutic drugs or biochemical tools. Here, we reported the discovery of highly selective and irreversible inhibitors of lipoprotein-associated phospholipase A2 (Lp-PLA2) using a covalent-fragment-based approach. The crystal structure of Lp-PLA2 in complex with a covalent fragment not only reveals the covalent reaction mechanism but also provides a good starting point to design compound **8**, which has a more than 130,000-fold and 3,900-fold increase in potency and selectivity, respectively, compared to those of the covalent fragment. Furthermore, fluorescent probes with high selectivity and sensitivity are developed to characterize Lp-PLA2 and its enzymatic activity *in vitro* or even in living cells in a way more convenient than immunoblotting test or immunofluorescence imaging. Overall, we provide a paradigm for application of the covalent-fragment-based strategy in covalent ligands discovery and the advantage of the enol-cyclocarbamate as a new warhead in designing covalent inhibitors of serine hydrolases.

INTRODUCTION

Traditionally, a covalent modification strategy has been regarded as a liability in pharmaceutical industry, mainly due to the safety concern, such as the possibility of non-specific binding, haptenization and possible idiosyncratic drug reactions.[1] Nevertheless, considering the therapeutic benefits of extended duration of action, increased potency or binding efficiency and binding to otherwise “intractable” targets, covalent ligands are of interest as therapeutic drugs.[2] In addition, covalent ligands are frequently used as biochemical tools for selective covalent modification of a target protein, in particular using activity-based protein profiling (ABPP),[3, 4] providing a powerful[5] and applicable way to characterise proteins and their functions.[6, 7]

To date, a number of covalent ligands (e.g. aspirin, penicillin, omeprazole, clopidogrel, neratinib etc.) have been approved as treatments for diverse clinical indications, making a significant impact on human health.[8] However, these drugs identified in natural products[9] were unexpectedly resulted from high-throughput screening campaigns.[2]

Recently, several strategies have been developed to design covalent ligands. For example, the choice of a highly reactive cysteine rather than lysine, serine or tyrosine of targeted proteins as the covalent site could efficiently form covalent bonds to compounds with otherwise low reactivity, resulting in significantly decreased risk of promiscuous protein labeling.[2] Moreover, mimicking the intermediate state in the chemical reaction (i.e. mechanism-based covalent inhibitors, Figure 1A) or directly adding reactive groups, often named covalent warheads, to highly selective reversible ligands (Figure 1B) rather than starting from a covalent fragment (Figure 1C) is generally used to derive potency and selectivity of resulting covalent ligands.[2, 10-13] With these strategies, several purposely designed inhibitors covalently attaching to a specific cysteine of protein kinases have been approved as drugs in recent years,[14] highlighting the utility and feasibility of irreversible ligand design. Other strategies, such as DNA-encoded libraries featuring electrophilic ligands, can also be used to develop covalent ligands, although examples of such applications are sparse.[1]

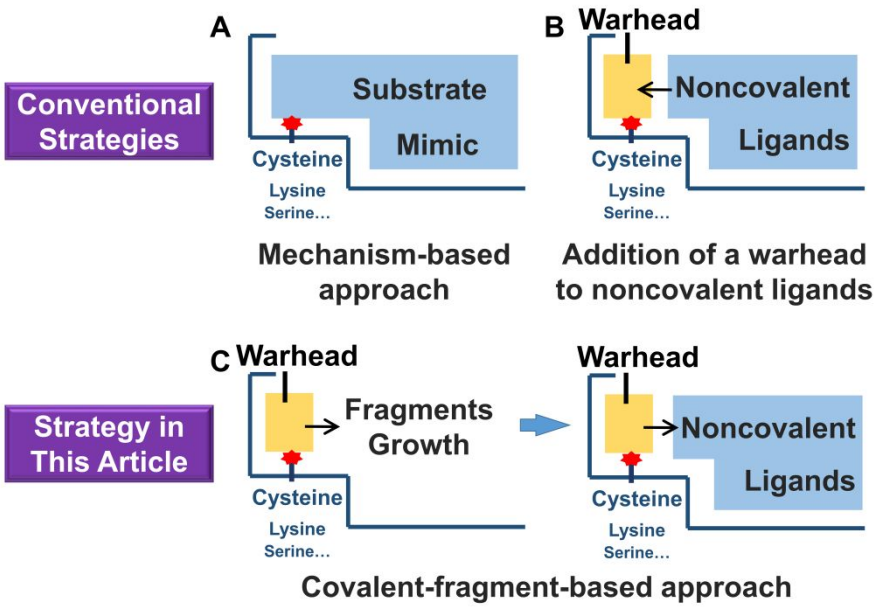

Figure 1. The strategies of covalent ligand design.

Although successful application has been achieved in targeting cysteine in protein kinases, these approaches are not suitable in every case of covalent ligands design. Covalent inhibitors design targeting lipoprotein-associated phospholipase A2 (Lp-PLA2, UniProt accession code: Q13093), a serine phospholipase belonging to group VII of PLA2 super-family, is exactly the case. This enzyme degrades certain oxidized phospholipids (oxPLs) which are resulted from the oxidative attack on phospholipid components of cellular membranes and lipoproteins into proinflammatory products, such as lysophosphatidylcholine (lysoPC) and oxidized nonesterified fatty acids (oxNEFA).[15] Lp-PLA2 is considered to be closely related to vascular inflammation and the FDA had

approved a reagent for measuring the Lp-PLA2 activity to identify individuals at higher risk of cardiovascular disease events.[16] Furthermore, Lp-PLA2 inhibitors have been studied for treating inflammation-related diseases, such as coronary heart diseases,[15] Alzheimer's disease[17, 18] and diabetic macular edema.[19-21] However, darapladib (**1**), an Lp-PLA2 inhibitor, was unable to meet its primary end points in phase III clinical trials on coronary heart diseases.[22, 23] In this context, designing covalent Lp-PLA2 inhibitors with higher potency and selectivity may be beneficial to take full advantages of the superiority of covalent drugs. In addition, the covalent inhibitor also could be used to develop specific probes as biochemical tools for elucidating functional versatility of the enzyme.

Given that serine and cysteine are the two most common covalent targeting residues, the catalytic serine (S273), which is the only serine within the substrate binding pocket of Lp-PLA2, could serve as an ideal covalent site. However, S273 is deeply located inside the pocket (Figure S1A) and most of the potent reversible inhibitors completely occupied the area around S273 (Figure S1B-F), leading to little space left for placement of an additional warhead. It is thus inappropriate to form a covalent bond with S273 by directly adding a warhead to known reversible inhibitors. Alternatively, replacing part of the non-

covalent inhibitors with various warheads might be an option, whilst it is not easy to keep the binding pose of the inhibitors before and after the replacement, and to ensure that the introduced warhead is able to form a covalent bond with S273. Therefore, the aforementioned strategies are not suitable to design the covalent inhibitors of Lp-PLA2 and another strategy is required. In addition, although a series of reversible Lp-PLA2 inhibitors have been disclosed,[15, 24] covalent inhibitors with high selectivity for Lp-PLA2 over PLA2VIIB have not been reported. PLA2VIIB, a homologous protein of Lp-PLA2, has a sequence identity of 41% and a conserved catalytic site to Lp-PLA2, resulting in a very similar substrate specificity of the two enzymes.[15] Therefore, the high selectivity of a covalent inhibitor towards Lp-PLA2 over PLA2VIIB should be considered.

Fragment-based lead discovery (FBLD) is a powerful approach for efficient discovery of novel ligands that regulate protein functions.[25] With the wide and successful application of FBLD strategy in non-covalent ligand development,[26] this strategy was also explored to design covalent ligands. Some covalent fragment screening efforts have been made recently[27-32] and a successful example is to design ligands covalently binding to the non-catalytic cysteine in protein kinases.[33] However, to the best of our knowledge, application

of the covalent-fragment-based approach to discover potent covalent ligands targeting serine has not been exemplified. This phenomenon is mainly caused by the concern that covalent fragments must have relatively high reactivity to gain a reactivity-driven affinity rather than a reversible binding affinity, resulting in subsequent bad selectivity.[34, 35] Here, we utilize a covalent-fragment-based approach (Figure 1C) to design covalent Lp-PLA2 inhibitors and select an applicable covalent fragment binding to S273 of Lp-PLA2 at the beginning. With the aid of multiple crystal structures, we quickly fill the remaining space of the substrate binding pocket and grow the fragment into a covalent Lp-PLA2 inhibitor with encouraging potency and selectivity. A further modification on this covalent inhibitor generates Lp-PLA2-specific fluorescent probes with high selectivity and sensitivity, which are useful to evaluate the binding efficiency of competitive ligands and label Lp-PLA2 *in vitro* or in living cells. These probes could also help to elucidate unexplored functions of the enzyme in future studies.

RESULTS

The choice of a covalent fragment/warhead. Given a relatively weak reactivity of serine compared to cysteine in the enzymes,[2] we initially sought a covalent warhead from known covalent ligands to ensure the formation of a covalent bond to S273. Among the published Lp-PLA2 inhibitors, SB-222657 (**2**),[36] JMN4 (**3**)[37] and SB-253514 (**4**)[38] were suggested to covalently binding to Lp-PLA2 (Figure 2A). However, the detailed covalent binding modes of these ligands with the enzyme are not known yet. In contrast to the extensive studies of β-lactam (a core of **2**) and carbamate (a core of **3**) covalent moieties in antibiotics and probes, respectively,[39, 40] the novel enol-cyclocarbamate covalent moiety (core of **4**) is rarely investigated. **4** is a natural product isolated from *Pseudomonas fluorescens* (DSM 11579) and was studied for antibiotics discovery with a focus on its Z-isomer.[41] It shows an inhibitory activity against Lp-PLA2 with an IC_{50} of 51 nM and also shows good selectivity for Lp-PLA2 over a range of other serine proteases, such as porcine elastase, trypsin, chymotrypsin, thermolysin, fungal aspartic protease, bacterial type IX metalloprotease, and the herpes protease enzymes.[38] Furthermore, the enantiomer of the chiral warhead of **4** has been successfully synthesized and confirmed to be hydrolytically stable.[42, 43] However, several issues of the enol-cyclocarbamate

scaffold remain to be addressed. First, the accurate covalent binding mechanism of the enol-cyclocarbamate with Lp-PLA2 is still unrevealed. The cyclocarbamate (C3) and the α,β-unsaturated carbonyl groups (C1), are possible electrophiles for S273 (Figure 2A). Second, the enol-cyclocarbamate derivatives have poor selectivity for Lp-PLA2 over PLA2VIIB. The IC_{50} of **4** for Lp-PLA2 is a 9-fold of the IC_{50} for PLA2VIIB.[38] Given the good selectivity of **4** for Lp-PLA2 over other serine hydrolases, unsolved problems with the enol-cyclocarbamate series as Lp-PLA2 inhibitors and the novelty of this warhead derived from a natural product, we decided to focus on the enol-cyclocarbamate warhead. In parallel, we tested the β-lactam and carbamate warheads using compounds SB-222657 (**2**) and JMN4 (**3**) as representatives but were unable to successfully determine their co-crystal structures with Lp-PLA2. Such a failure might be due to a low solubility of these two compounds in aqueous solution (**2**, cLogP: 5.5; **3**, cLogP: 6.6).

Characterization of the enol-cyclocarbamate warhead reacting with Lp-PLA2. It has been reported that the stereochemistry of the chiral carbon at the ring junction is not critical to the Lp-PLA2 inhibition.[42] Following the reported synthesis route,[42] we first

synthesized fragment **5**, an enantiomer of the chiral warhead in **4**. The enzymatic assay shows that this fragment has a millimolar inhibitory activity against both Lp-PLA2 and PLA2VIIB with no selectivity (Figure 2A). We also determined a co-crystal structure of Lp-PLA2 bound with **5** (PDB code: 6M06) to provide structural insight into the reaction mechanism of this type of warhead (Figure 2B). Contiguous electron density was clearly shown between S273 and **5**, strongly implying the formation of a covalent bond, and allowed to exactly place a covalent bond between the hydroxyl oxygen of S273 and the C3 but not C1 atom of fragment **5**.

Based on this crystal structure, a presumed mechanism of **5** reacted with Lp-PLA2 is shown in Scheme 1. In brief, an acylation reaction proceeds through the nucleophilic addition of the hydroxyl oxygen of S273 to the carbonyl carbon (C3) of fragment **5**, simultaneously facilitated by proton transfer from S273 to H351, which serves as a base, resulting in a tetrahedral intermediate. Through H-bonding interactions, the major role of the oxyanion hole formed by NH groups of F274 and L153 is to stabilize the negative-charged tetrahedral intermediate. From the intermediate to products, a proton transfers from H351 to the oxygen linked to C1 of **5** and the breakage of the scissile bond happens

spontaneously. In addition, the terminal carboxyl group of the covalently bound fragment H-bonds to Q352, and the pyrrolidine moiety forms hydrophobic interactions with W298, F322 and H351 (Figure 2B).

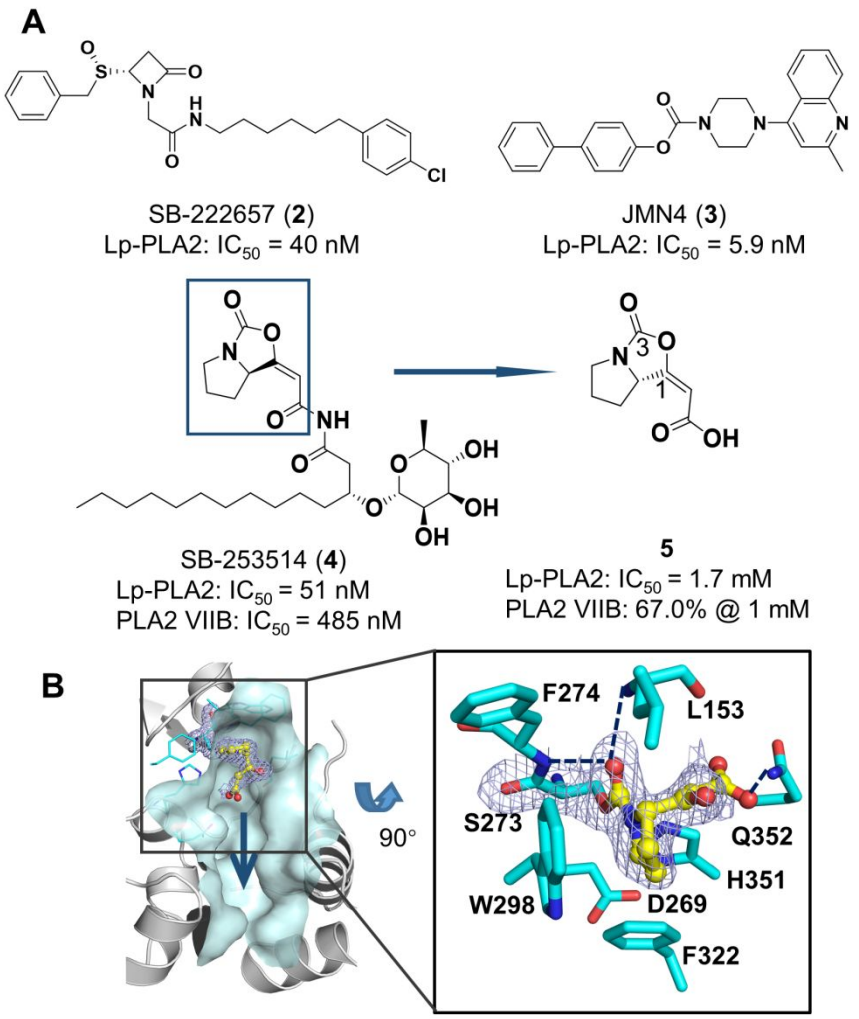

Figure 2. Covalent binding of the enol-cyclocarbamates to Lp-PLA2. (A) Structures of three suspected covalent inhibitors of Lp-PLA2 and fragment **5**. The inhibition of fragment **5** against Lp-PLA2 and PLA2VIIB was shown under the structure. (B) A co-crystal

structure of fragment **5** covalently bound to Lp-PLA2 (PDB code: 6M06). The direction for fragment **5** to grow into a more potent ligand is shown by a blue arrow. A close-up view of the binding pocket, in which fragment **5** (yellow) together with surrounding residues (cyan) are shown as sticks and H-bonds are represented by dashed lines. The mesh depicts the ($2F_o$-F_c) difference electron-density maps of the fragment contoured at 1.2 σ.

Scheme 1. A presumed mechanism for the reaction of fragment 5 with catalytic residues of Lp-PLA2 based on the crystal structure of Lp-PLA2 in complex with 5.

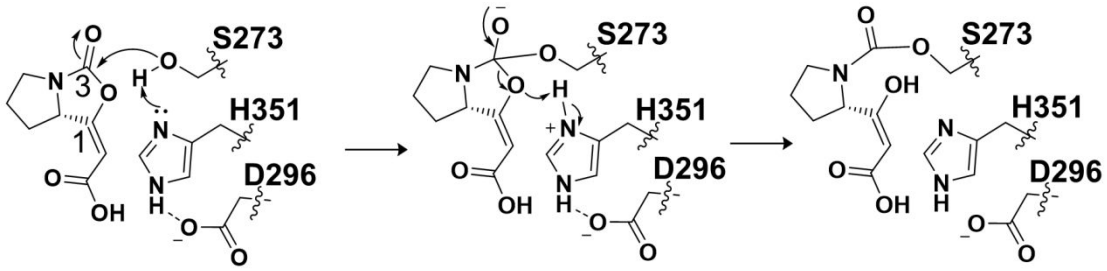

A low reactivity of the enol-cyclocarbamate towards cysteine. Since fragment **5** can covalently modify the catalytic serine of Lp-PLA2, it is also possible to react with cysteine, thereby resulting in unexpected covalent modification. It is thus important to explore the electrophilicity and lability of fragment **5** targeting cysteine. We measured the half-life for the reaction of **5** with glutathione (GSH $t_{1/2}$), which is widely used to mimic proteinaceous

cysteine reactivity.[30, 44] To determine the rates of reaction with GSH, the N-phenyl acrylamide (a positive control) or fragment **5** was incubated with GSH, and the remaining GSH at varying time after incubation was determined. The GSH $t_{1/2}$ of the N-phenyl acrylamide is 285 min which is close to the reported value and for fragment **5** it is 1888 min, which is longer than most available warheads targeting cysteine and some approved covalent drugs (Figure S2).[45] This result demonstrates that the enol-cyclocarbamate warhead shows low reactivity towards cysteine, suggesting the low probability of non-specific binding to cysteine.

A fusion of the covalent enol-cyclocarbamate and darapladib. As shown in Figure 2B with a blue arrow, the complex structure also revealed that the terminal carboxyl group of fragment **5** offers a perfect growth vector towards the unoccupied pocket which is exactly the binding pocket for reversible inhibitors, providing a great opportunity for fragment evolution in the next step. Subsequently, to accelerate the growth of fragment **5**, we overlaid the crystal structures of Lp-PLA2 in complex with fragment **5** as well as previously reported non-covalent inhibitors to dig out a suitable scaffold fitting well into the unoccupied pocket. To our delight, we found that the biphenyl ethanediamine moiety

(fragment **6**) of darapladib, the blue part shown in Figure 3A, could be a good candidate, as the amide group of darapladib is proximal to the carboxyl group of **5** bound in Lp-PLA2 (a red circle shown in Figure 3A). Given that darapladib possesses superb Lp-PLA2 inhibitory potency (IC_{50}: 0.7 nM) and decent selectivity (1,200-fold) against PLA2VIIB,[46] we designed and synthesized compound **7** in which fragment **5** is fused into darapladib based on the superimposition of two complex structures. Surprisingly, compound **7** not only gains a high inhibitory activity against Lp-PLA2 with an IC_{50} of 25 nM, ~68,000-fold improvement compared to **5**, but also exhibits more than 1,000-fold selectivity for Lp-PLA2 over PLA2VIIB (Figure 3A). In addition, compound **7** showed a time-dependent inhibition on Lp-PLA2, indicating the irreversible binding feature as expected. A plot of the observed rates of inhibition (k_{obs}) of **7** against Lp-PLA2 versus concentration revealed a k_{inact}/K_I value of 3140 $M^{-1}\cdot s^{-1}$, which is a typical sign for an irreversible inhibitor (Figure S3A and S3B). A protein mass spectrometry analysis confirmed the covalent adduct of Lp-PLA2 with a mass matching that of the wild-type enzyme modified by a condensation with one molecule of compound **7** (Figure S4). We further solved the co-crystal structure of compound **7** bound to Lp-PLA2 (PDB code: 6M08), and found that only one molecule

of **7** covalently binds to S273 and no extra unfilled electronic density left behind. This is consistent with the results from the enzymatic activity assay and the mass spectrometry analysis, showing that compound **7** reacted with Lp-PLA2 with 1:1 stoichiometry.

The crystal structure of the Lp-PLA2-**7** complex revealed that the enol-cyclocarbamate warhead of **7** adopts a highly conserved binding pose of fragment **5** and the covalent bond is exactly maintained (Figure 3B). Moreover, the biphenyl group of **7** inserts into a hydrophobic sub-pocket formed by L371, L369, F357, A355, Q352, G154, L121, L111, and F110, while the ethanediamine moiety extends to the solvent region. The crystal structures of Lp-PLA2 in complex with compound **7** superimposed on darapladib demonstrate that the protein-ligand interaction patterns of the biphenyl ethanediamine moiety in two complexes are highly conserved (Figure 3C). Therefore, in the Lp-PLA2-**7** complex, both the warhead which is almost identical to fragment **5** and the non-covalent interacting portion borrowed from darapladib bind to the pocket as we desired (Figure 3D), highlighting the power and advantage of the structure-based drug design strategy. Notably, although compound **7** selectively inhibited Lp-PLA2 at a nanomolar concentration, both the warhead (fragment **5**) and the biphenyl ethanediamine moiety

(fragment **6**) showed extremely weak potency and low selectivity. Inhibition of fragment **6** on Lp-PLA2 is only 43% at a concentration of 200 μM, and it is 44% for PLA2VIIB at a concentration of 250 μM (Figure 3A). It is thus suggested that contribution of the enol-cyclocarbamate warhead and the reversible fragment **6** has a significantly synergetic effect on the potency and selectivity improvement.

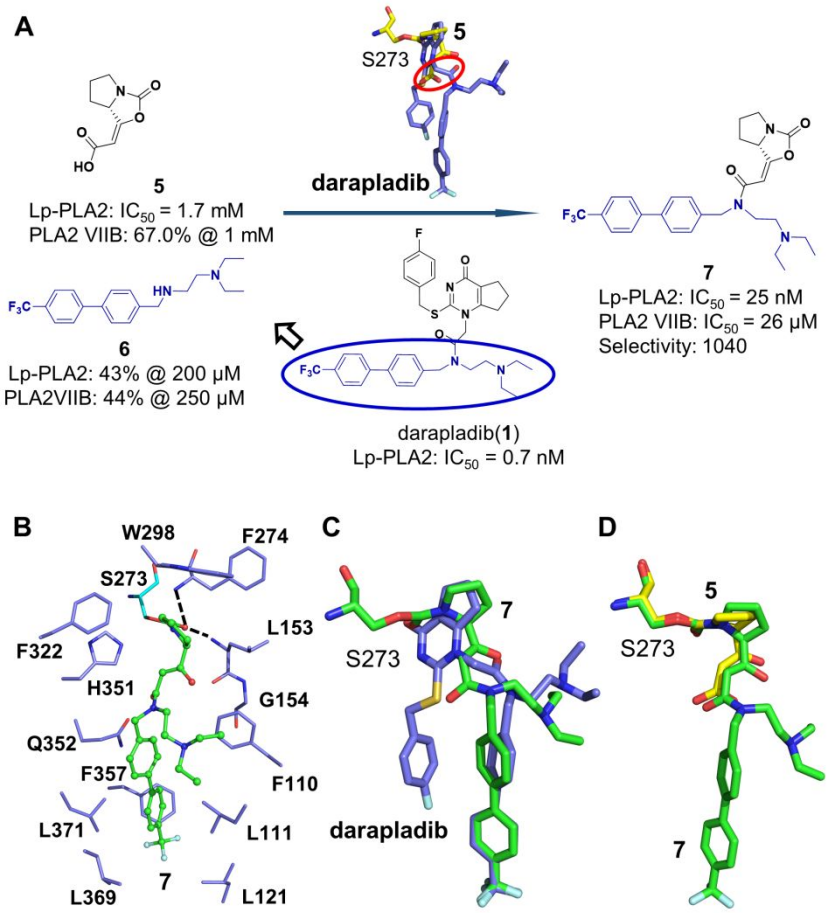

Figure 3. The discovery of compound **7** by a fusion of the covalent enol-cyclocarbamate and darapladib. (A) Schematic description for the design of compound **7** based on

fragment **5** and darapladib. A red circle indicates the proximity between the amide of darapladib and the carboxyl of **5** by superimposing the co-crystal structures of Lp-PLA2 in complex with **5** (yellow) and darapladib (blue). (B) The Lp-PLA2-**7** complex structure reveals interactions of **7** (green) with residues (blue) in the substrate binding pocket (PDB code: 6M08). H-bonds are represented by dashed lines. (C, D) Structure superimposition of Lp-PLA2-**7** on Lp-PLA2-darapladib (C) or Lp-PLA2-**5** (D).

Introduction of a substituent filling into an unoccupied sub-pocket. After a thorough investigation on the complex structure of Lp-PLA2-**7**, we considered an unoccupied sub-pocket formed by L107, A155, L159, A355, and F357 near the trifluoromethyl substituted benzene ring of the biphenyl group. Substituents at the meta-position of the trifluoromethyl on this benzene ring might occupy this hydrophobic sub-pocket (Figure 4A-B). Accordingly, we introduced a linear and a cyclic lipophilic substituent in compounds **8** and **9**, respectively, in order to fill the sub-pocket (Figure 4 and Figure S5). The enzymatic activity assay demonstrated that a linear 1,1,1-trifluoroethoxyl group introduced in compound **8** enhanced ~2-fold inhibitory potency to IC_{50} = 13 nM. The k_{inact}/K_I value of compound **8** (6835 $M^{-1}\cdot s^{-1}$) also showed ~1-fold increase compared to **7**

(Figure S3C and S3D). Most importantly, the selectivity of **8** for Lp-PLA2 over PLA2VIIB reaches ~3,900-fold (Figure 4A), which is almost four times that of **7** (~1040-fold). Compound **8** is by far the most selective inhibitor of Lp-PLA2 to the best of our knowledge. The determined crystal structure of compound **8** in complex with Lp-PLA2 (PDB code: 6M07) revealed the conserved protein-ligand interactions as those presented in the co-crystal structure of Lp-PLA2-**7** except that the hydrophobic sub-pocket mentioned above was perfectly occupied by the substituted 1,1,1-trifluoroethoxyl group at the terminal benzene ring of **8** (Figure 4B). By comparison, compound **9**, introducing a benzyloxy group at the same position, showed a similar potency compared to **8**, while its selectivity for Lp-PLA2 over PLA2VIIB dramatically declines to ~360-fold (Figure S5). The reason for such a drop in selectivity from **8** to **9** is that **9** is a more potent inhibitor of PLA2VIIB, but the mechanism of action of the substituted benzyloxy group on PLA2VIIB remains unknown.

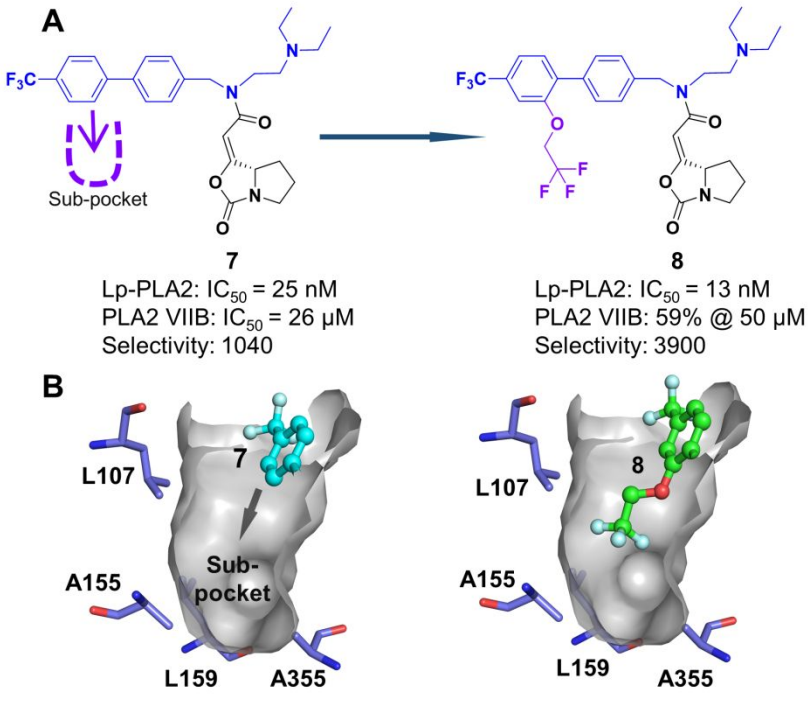

Figure 4. The discovery of compound **8** with high potency as well as selectivity for Lp-PLA2 over PLA2VIIB. (A) Schematic description for structure-based optimization of compound **7** to yield compound **8**. (B) The co-crystal structures of Lp-PLA2-**7** and Lp-PLA2-**8** (PDB code: 6M07) complexes, in which a sub-pocket marked with a gray arrow was perfectly occupied by the introduced trifluoro-ethoxyl group.

High selectivity of compound 8 for Lp-PLA2 over other serine hydrolases. Because of the concerns of nonspecific or off-target adduct formation, selectivity is one of the key issues in design of safe and effective covalent ligands. It is especially important for inhibitors of serine hydrolases like Lp-PLA2, due to the existence of a huge number of

these enzymes in cells.[47] With these considerations in mind, we applied the activity-based protein profiling (ABPP) method to investigate the selectivity of compound **8** in HEK293T cells.[37] ABPP mainly utilizes the active-site directed covalent probes to target specific one or subsets (families) of proteins in complex proteomes so as to provide a quantitative readout of the functional state of the targeting protein(s).[4] The gel-based competitive ABPP analysis was performed using FP-TAMRA which is a non-selective covalent fluorescent probe of serine hydrolases. We first incubated the HEK293T lysate with compound **8** at different concentrations and then added FP-TAMRA to the lysates. An in-gel fluorescence scanning was performed on samples, showing that compound **8** did not cross react with other serine hydrolases at concentrations up to 50 μM (Figure 5). Presumably overlapped by other enzymes, a small amount of the basal Lp-PLA2 in the HEK293T cell was not clearly visualized in the gel. To highlight the band of Lp-PLA2, we repeated the same experiment with the HEK293T lysate added with the recombined human Lp-PLA2 which was also used in other experiments involved in this study, distinctly showing the changes of the Lp-PLA2 band before and after adding **8** at different

concentrations (Figure 5). It is thus concluded that compound **8** has an excellent selectivity for Lp-PLA2 over other serine hydrolases in the cells.

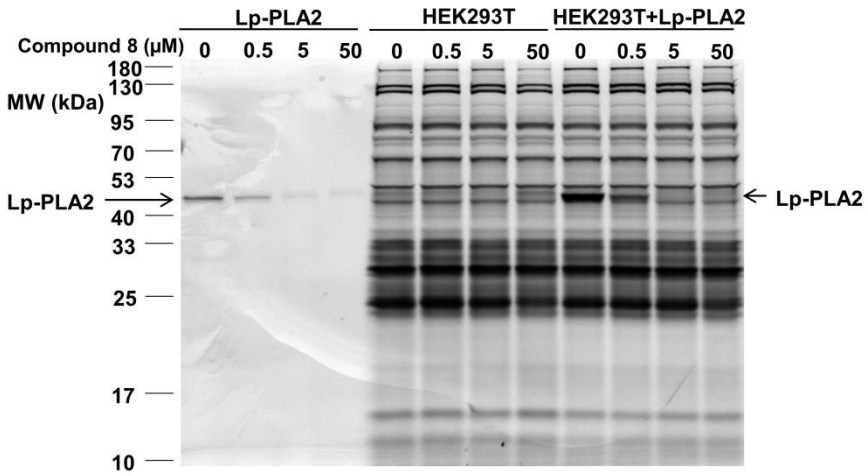

Figure 5. Selectivity evaluation of compound **8** in cells by the gel-based competitive ABPP probed with FP-TAMRA which is a non-selective covalent fluorescent probe of serine hydrolases. By comparison, the recombined human Lp-PLA2, the HEK293T lysate and the mixture of these two were used in the first, second and third four samples, respectively, and an in-gel fluorescence scanning was performed on all the samples.

Fluorescent probes design based on compound 8. Inspired by the excellent selectivity of compound **8** in HEK293T cells, we decided to label compound **8** with different fluorescent groups so as to provide an ideal fluorescent probe for Lp-PLA2. According to the co-crystal structure of Lp-PLA2-**8**, the ethanediamine moiety is exposed to the solvent

accessible region and is thereby an ideal site to attach fluorophores without interfering with the inhibitory activity. Utilizing difluoroboron dipyrromethene and lissamine rhodamine B as the luminophore, we designed and synthesized two fluorescent compounds, **8-BODIPY** and **8-RH**, respectively (Figure 6A), based on compound **8**. The enzymatic activity assay showed that two fluorescent compounds maintain the nanomolar potency against Lp-PLA2 (**8-BODIPY**: IC_{50} = 14 nM; **8-RH**: IC_{50} = 25 nM). The gel-based fluorescent labelling analysis with **8-BODIPY** or **8-RH** shown in Figure S6 revealed that these two fluorescent compounds hardly label any other proteins except Lp-PLA2 and its degradation at concentrations up to 5 μM, which is ~385-fold and 200-fold of the *in-vitro* IC_{50}s of **8-BODIPY** and **8-RH**, respectively. This again manifests the excellent selectivity of the two fluorescent probes and their parent compound (**8**). An immunoblotting test on the same gel used for fluorescence scanning resulted in the bands identical to the fluorescent bands, demonstrating that the selectivity and sensitivity of our fluorescent probes are comparable to the antibody of Lp-PLA2 (Figure S6).

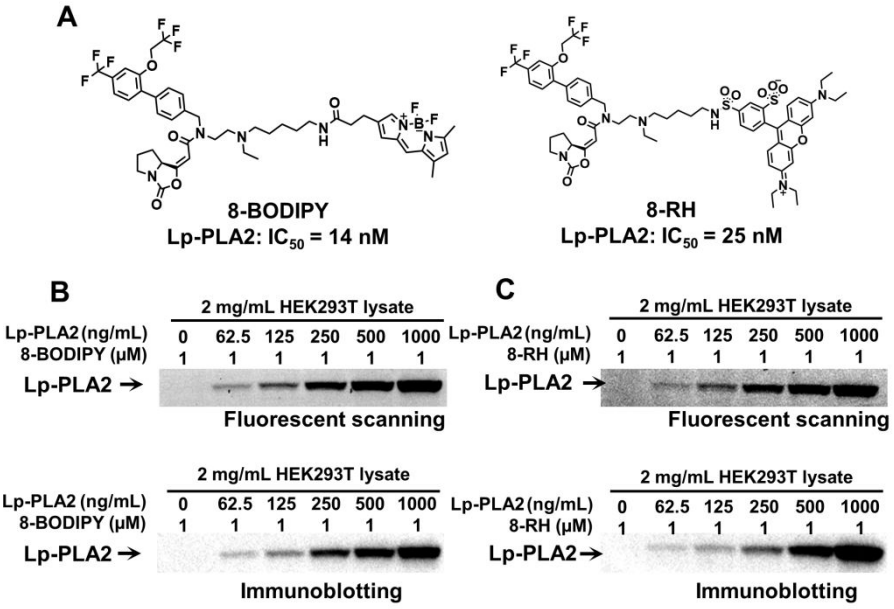

Figure 6. (A) Chemical structures of **8-BODIPY** and **8-RH**. (B, C) An in-gel fluorescence scanning using **8-BODIPY** (B) or **8-RH** (C) as a fluorescent probe with the HEK293T lysate added with different concentrations of recombinant human Lp-PLA2. An immunoblotting test was performed on the same gel used for the fluorescence scanning.

Fluorescent labeling of Lp-PLA2 by 8-BODIPY and 8-RH. With the high potency and selectivity, **8-BODIPY** and **8-RH** are capable of specifically modifying Lp-PLA2 or qualitative and even semi-quantitative characterization of the enzyme. We incubated the two probes with the HEK293T lysate added with different concentrations of recombinant human Lp-PLA2, an in-gel fluorescence scanning was then performed on samples, and

eventually an immunoblotting test was carried out on the same gel used for the fluorescence scanning (Figure 6B and 6C). With a more convenient way, the bands, which qualitatively and semi-quantitatively label Lp-PLA2 in the lysate, resulted from the in-gel fluorescence scanning are highly consistent with those from the immunoblotting test.

In addition, **8-BODIPY** or **8-RH** can also be used as an activity-based probe for profiling Lp-PLA2 inhibited by a competitive binding ligand. The gel-based competitive ABPP analysis of compound **8** with the use of **8-BODIPY** and **8-RH** as probes confirmed the inhibition of Lp-PLA2 by **8**, which is not accessible by the immunoblotting test (Figure S7).

Then the probes were tested in HEK293T cells which were transfected with the Lp-PLA2 expression vector. Due to a poor solubility and membrane permeability of **8-RH**, only **8-BODIPY** was tested. HEK293T cells were transfected with Lp-PLA2 and cultured for 48 h followed by the incubation with 1 μM **8-BODIPY** for 10 min. Then the cells were collected for SDS-PAGE followed by the in-gel fluorescent scanning which showed a distinct band of Lp-PLA2 (Figure S8). An immunoblotting test on the same gel resulted in

the bands identical to the fluorescent bands, demonstrating the labelling of endogenous Lp-PLA2 by **8-BODIPY** (Figure S9).

Florescence polarization-based competitive experiment between 8-BODIPY and darapladib. To investigate the competitive binding of our covalent inhibitors versus non-covalent inhibitors to Lp-PLA2, an experiment of competition between **8-BODIPY** and darapladib was performed with a fluorescence polarization-based assay, as the fluorescent probe, **8-BODIPY**, is derived from the covalent inhibitor **8**. Darapladib is the most potent non-covalent inhibitor of Lp-PLA2 with an IC_{50} of 0.7 nM and thus was used for this experiment. Recombinant Lp-PLA2 was first incubated with gradiently diluted darapladib followed by an addition of 10 nM **8-BODIPY**, and the signal of fluorescence polarization decreased with the increased concentration of darapladib (Figure S10). This result reveals that the half maximal competitive concentration of darapladib is 11.65 nM in the presence of 10 nM **8-BODIPY**, demonstrating the competition between **8-BODIPY** and darapladib. In contrast, the signal of fluorescence polarization only slightly changed with the increased concentration of darapladib (Figure S10) when recombinant Lp-PLA2 was first incubated with 10 nM **8-BODIPY** followed by the addition of gradiently diluted

darapladib. These results show an irreversible binding of **8-BODIPY** to Lp-PLA2 and reveal that the higher binding ability of the covalent inhibitors allows them to compete for potent non-covalent inhibitors.

Fluorescence imaging of 8-BODIPY in living cell. Next, **8-BODIPY** was tested for live-cell imaging. Living PC-3 cells, in which the endogenous Lp-PLA2 is expressed, were treated with **8-BODIPY**, ER-Tracker Red and Hoechst 33342 which characterizes Lp-PLA2, endoplasmic reticulum (ER) and nucleus, respectively, for a confocal laser scanning. The resulting imaging shows colocalization of fluorescence of **8-BODIPY** and ER-Tracker Red (Figure S11), suggesting Lp-PLA2 tends to co-localize with ER. Such a result is consistent with the characteristic of secreted proteins like Lp-PLA2[48] and matches an immunofluorescence imaging of Lp-PLA2 in a previous work.[49]

To further confirm the binding of **8-BODIPY** with Lp-PLA2 in the living cells, an experiment of competitive binding with Lp-PL2 between **8-BODIPY** and darapladib was performed. The result showed that the florescent signal of **8-BODIPY** within cells decreased after the competitive binding of darapladib with Lp-PLA2 (Figure S12), demonstrating the binding of **8-BODIPY** with Lp-PLA2 in the living cells.

DISCUSSION AND CONCLUSIONS

In summary, to accomplish the evolution of a covalent fragment/warhead into a potent and selective ligand, we efficiently conducted two rounds of optimization and synthesised compounds with the aid of the co-crystal structures. The resulting compound **8** has a more than 130,000-fold increase in the inhibitory activity on Lp-PLA2 and a 3,900-fold increase in the selectivity for Lp-PLA2 over PLA2VIIB. It is by far the most selective inhibitor of Lp-PLA2. Furthermore, it shows an excellent selectivity over a wide range of other serine hydrolases in the cells, providing a qualified covalent lead for further development. Future studies are warranted to evaluate the potency of compound **8** against Lp-PLA2 *in vivo* as well as the efficacy of the compound in the animal models for Lp-PLA2-related diseases. Additionally, based on this compound, we designed selective and sensitive Lp-PLA2 probes to characterize Lp-PLA2 *in vitro* or even in living cells in a more convenient way, and also to be used as probes of ABPP tailored for Lp-PLA2. Based on these results, these probes could be considered as a useful chemical biology probe

that might help understanding the role of Lp-PLA2 in physiological and pathophysiological conditions.

It is noteworthy that our work presented here used a covalent-fragment-based approach to successfully discover serine-targeted covalent ligands. As a result, we efficiently obtained a covalent inhibitor of Lp-PLA2 with an outstanding selectivity and potency from a covalent warhead (fragment **5**) and a reversible fragment (fragment **6**) which is derived from a well-known reversible inhibitor by crystal structures superimposition, although both fragments have extremely weak selectivity as well as potency. It is thus manifested that the covalent-fragment-based lead discovery could be utilized as a feasible way complementary to the conventional approaches used for design of covalent drugs or probes, especially when the warhead cannot be directly added to reversible ligands.

EXPERIMENTAL SECTION

Chemistry. Fragment **5** was resulted from the deprotection of the intermediate **5a**, which was described in the literature.[42] Compound **6** was obtained following the synthetic

route reported previously[50]. As shown in Scheme 2, compound **7** was synthesized according to the General Procedure C by using compounds **5** and **6** as the starting materials.

Scheme 2. Synthesis of compounds 5 and 7[a].

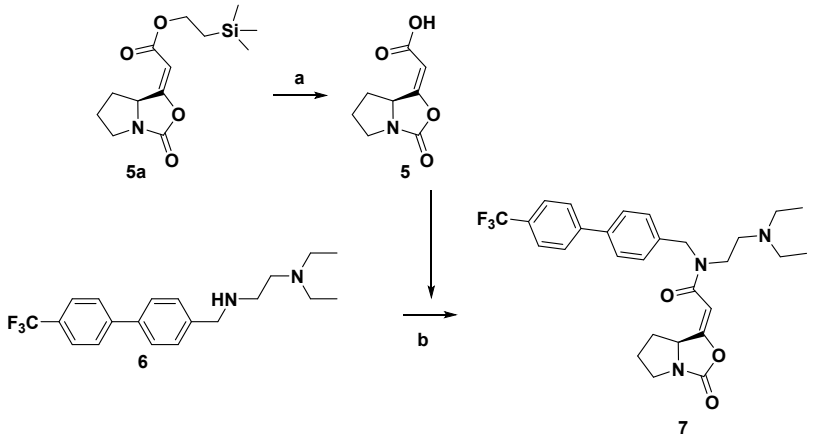

[a]Reagents and conditions : (a) THF, TBAF, 25 ℃, 16 h. (b) DMF, HATU, DIPEA, 25 ℃, 16 h.

Compounds **8** and **9** were synthesized according to Scheme 3. The intermediates **7a** and **7b** were obtained from coupled reactions between 4-formylphenylboronic acid and **6a** as well as **6b**, and were subsequently transformed into **8a** and **8b** after reductamination with *N*,*N*-diethylethylenediamine. **8a** and **8b** generated compounds **8** and **9** after a condensation reaction with fragment **5**.

Scheme 3. Synthesis of compounds 8 and 9[b].

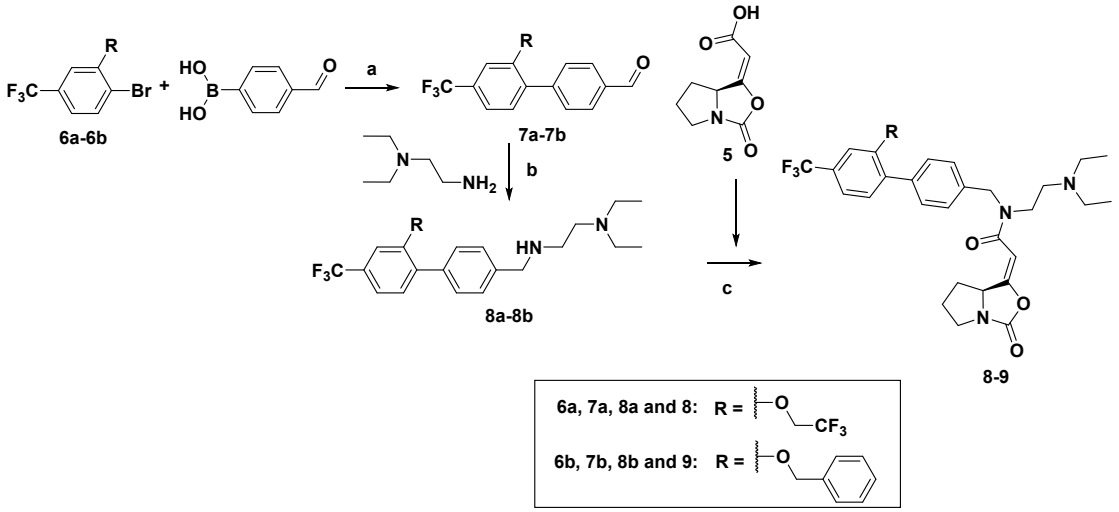

[b]Reagents and conditions : (a) toluene/methanol/water (v/v/v) = 2/1/1, Na_2CO_3, $Pd(PPh_3)_4$, 80 °C, 16 h; (b) DCM, activated molecular sieve (MS4A, graininess), 25 ℃, 16 h, then, MeOH, $NaBH_4$, 25 ℃, 30 min; (c) DMF, HATU, DIPEA, 25 ℃, 16 h.

Fluorescent probes **8-BODIPY** and **8-RH** were synthesized according to Scheme 4. The linker **13** were obtained from a deprotection of **12**, which was prepared from 2-(carbobenzoxyamino)-1-ethanol through protection, nucleophilic substitution and alkylation reactions. The pharmacophores **7a** and **5** were successively introduced to **13** by reductamination and condensation reactions, respectively. The resulting compound **15** was then transformed into **16** by a deprotection reaction. At last, the fluorophores, **17a**

and **17b**, were introduced by nucleophilic substitution and condensation reactions, respectively.

Scheme 4. Synthesis of fluorescent probes 8-BODIPY and 8-RH[c].

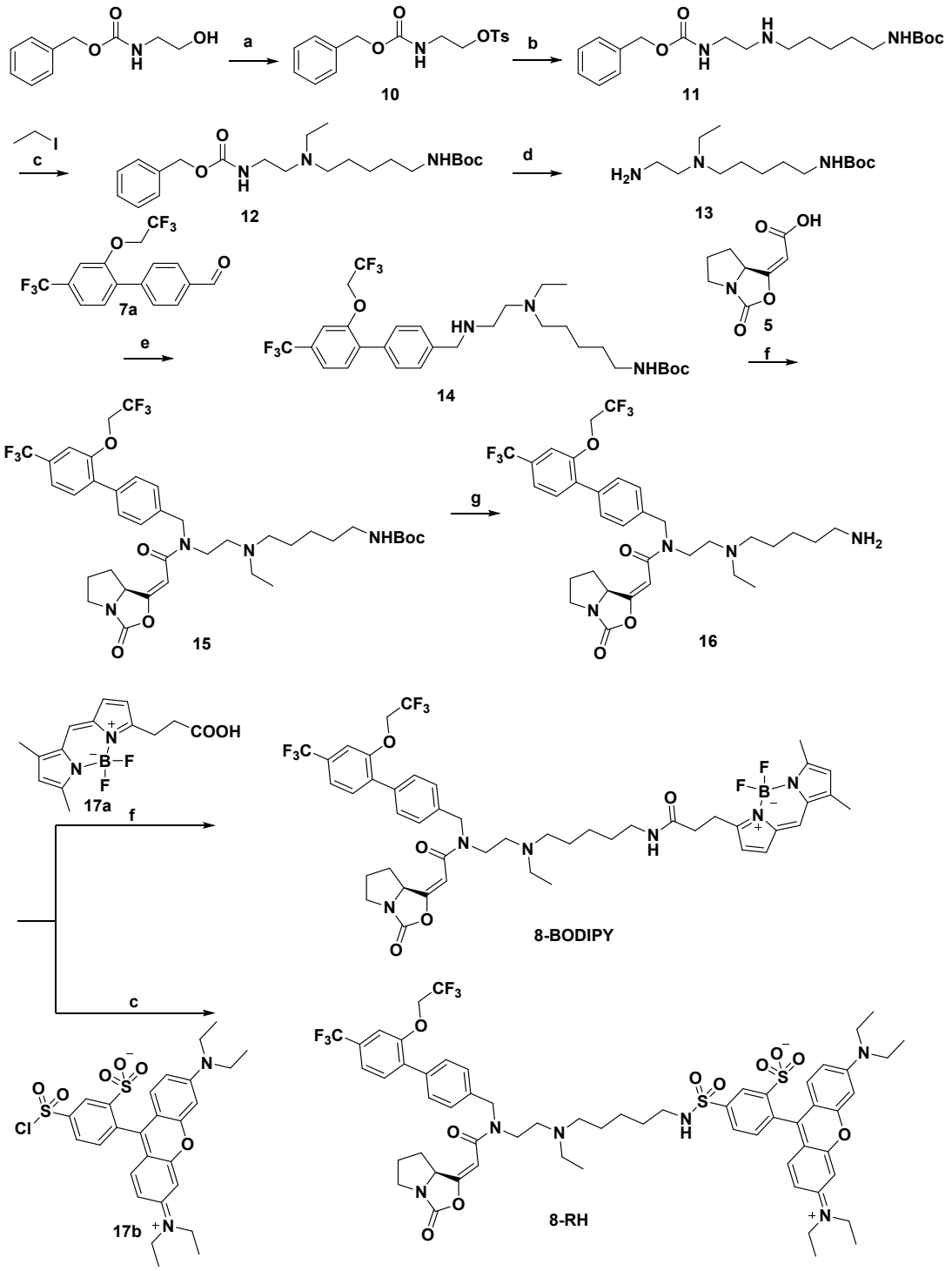

[c]Reagents and conditions : (a) DCM, TsCl, DMAP,Et_3N, 0℃ to 25 ℃, 5 h; (b) MeCN, *N*-Boc pentamethylene diamine, K_2CO_3, 50℃, 16 h; (c) DMF, DIPEA, iodoethane, 25 ℃,

16 h; (d) MeOH, Pd/C, H_2, 25 ℃, 16 h; (e) DCM, activated molecular sieve (MS4A, graininess), 25 ℃, 16 h, then, MeOH, $NaBH_4$, 25 ℃, 30 min; (f) DMF, HATU, DIPEA, 25 ℃, 16 h; (g) DCM/TFA (v/v = 5:1), 25 ℃, 16 h.

Enzymatic assay *in vitro*. The inhibitory activity of compounds against the human recombinant Lp-PLA2 or PLA2VIIB was measured according to the protocol of Chen et al.[51] The substrate 2-thio-PAF (Cayman Chemical) and 5,5'-dithiobis-(2-nitrobenzoic acid) (DNTB, Sigma-Aldrich) were used to produce the product with an absorbance at 412 nm. The recombinant was directly added to the enzymatic system: 5 μL of the compound, 10 μL of 10 mM DNTB, and 10 μL of protein were incubated for 30 min at 25 ℃. Finally, 175 μL of substrate solution (100 mM Tris pH 7.2, 1 mM EGTA, 50 μM 2-S-PAF) was added to the enzymatic system. Enzymatic kinetics were measured every minute of the reaction time (10 min in total), and an initial velocity was obtained to measure the inhibition. The IC_{50} curves were generated using GraphPad Prism, and each IC_{50} measurement was repeated at least three times.

Crystal structure determination. The purified protein was concentrated to 4 mg/mL for crystallization. Crystallization of Lp-PLA2 was carried out by mixing the protein with an

equal volume of the precipitant solution (0.1 M MOPS pH 6.6, 0.4 M Li_2SO_4, 27% (w/v) $(NH_4)_2SO_4$, 1 M Na-Ac, 1.4% (v/v) 1,4-butanediol). Crystals were obtained by the vapor-diffusion method in hanging drops at 20 °C.

Crystals of the Lp-PLA2-**5** complex were prepared by soaking crystals of apo Lp-PLA2 into the reservoir solution containing 50 mM fragments **5** for 16 h. Micro-seeding was used to obtain the crystals of Lp-PLA2 in complex with compound **7** or **8**. Crystals of the protein-compound complex were harvested in the mix of reservoir solution and 4 mg/mL Lp-PLA2 containing 1 mM compound **7** or **8** added with micro-seeds of apo Lp-PLA2 crystals. All crystals were directly flash frozen in liquid nitrogen before diffraction test.

Data were collected at 100 K at the Shanghai Synchrotron Radiation Facility (SSRF)[52] and were processed with the HKL software packages.[53] The structures were solved by molecular replacement, using the program PHASER[54] with the search model of PDB 5I9I. The structures were refined with the program PHENIX[55] and REFMAC5.[56] With the aid of the program Coot,[57] compounds and water molecules were fitted into the initial *Fo−Fc*

map. The complete statistics, as well as the quality of three determined structures, are shown in Table S1.

Gel-based competitive ABPP assays. HEK293T (human embryonic kidney) cells were cultured at 37 °C under 10% CO_2 in DMEM containing phenol red, stable glutamine, and 10% (v/v) Fetal Bovine Serum (Gibico). Cells were passaged at 80-90% confluence by resuspension in fresh medium. Cell pellets were thawed on ice, resuspended in cold lysis buffer (20 mM HEPES pH 7.2, 2 mM DTT, 250 mM sucrose, 1 mM $MgCl_2$, 2.5 U/mL benzonase) and incubated on ice (15-30 min). Cells were lysed with a probe sonicator, and diluted to 2 mg/mL in the lysis buffer. Protein concentrations were determined with the Bradford Protein Assay. Recombinant human Lp-PLA2, the HEK293T lysate (2.0 mg/mL) or the HEK293T lysate (2.0 mg/mL) added with the recombinant human Lp-PLA2 was pre-incubated with vehicle or inhibitor (0.5 μL 40 × inhibitor stock, 30 min, 37 ˚C) followed by an incubation with the activity-based probe, FP-TAMRA (Thermo Scientific™, 88318), **8-BODIPY** or **8-RH** at a concentration of 1 μM for 20 min at 37 ˚C. Final concentrations for the compound are indicated in the main text and figure legends. Reactions were quenched with Laemmli buffer. Samples were resolved on a 12.5%

acrylamide SDS-PAGE gel and visualized by in-gel fluorescent scanning (Typhoon FLA 9500, GE Healthcare, Figure 5 and Figure S7).

Fluorescent labeling of Lp-PLA2 by 8-BODIPY and 8-RH. HEK293T lysate (2.0 mg/mL) or HEK293T lysate (2.0 mg/mL) in addition with recombinant human Lp-PLA2 was incubated with different concentrations of **8-BODIPY** or **8-RH** (30 min, 37 ˚C). Reactions were quenched with Laemmli buffer. Samples were run on a 12.5% acrylamide SDS-PAGE gel and visualized by in-gel fluorescent scanning (Typhoon FLA 9500, GE Healthcare) followed by immunoblotting (Figure 6 and Figure S6).

For the experiment of endogenous Lp-PLA2 labelling, HEK293T cells were seeded in six-well plates and incubated for 16 h. The following day, cells were transfected with an Lp-PLA2 (47-429) expression vector using Lipofectamine 3000 (Life Technologies). After 48 h, cells were washed by Phosphate Buffered Saline (PBS) once followed by the addition of either **8-BODIPY** (1 μM) or **DMSO** as a control in PBS for 10 min. Cells were then collected for SDS-PAGE gel followed by in-gel fluorescent scanning (Typhoon FLA 9500, GE Healthcare) and immunoblotting (Figure S8 and S9).

Immunoblotting. Samples (20 μL) were denatured with Laemmli buffer was run on a 12.5% acrylamide SDS-PAGE gel. Proteins were transferred to 0.2 μm polyvinylidene difluoride membranes (Bio-Rad, 160177). Membranes were washed with TBS (50 mM Tris, 150 mM NaCl) and blocked with 5% bovine serum albumin (BSA) in TBS-T (50 mM Tris, 150 mM NaCl, 0.1% Tween 20) for 1 h at 25 ℃. Membranes were then incubated with the primary antibody (Human PLA2G7/PAF-AH/Lp-PLA2 Antibody, 1:2000, R&D Systems, AF5106-SP, Lot: CCDC041809A; GAPDH Rabbit mAb antibody, 1:5000, Cell Signaling Technology, 2118L, Lot: 10) in 5% BSA TBS-T for 16 h at 4 °C, washed with TBS-T, incubated with the secondary antibody (Rabbit anti-Goat IgG-HRP, 1:10000, absin, abs20005, Lot: #17; Peroxidase AffiniPure Goat Anti-Rabbit IgG (H+L), Jackson ImmunoResearch, 111-035-003, 1:10000, Lot: 146671) in 5% BSA TBS-T (1 h, 25 °C) and washed with TBS-T. Imaging solution (Tanon™ High-sig ECL Western Blotting Substrate, 180-501) was added to develop membranes and chemiluminescence was detected on the ChemiDoc (Bio-Rad) using standard chemiluminescence settings.

Florescence polarization-based experiment for exploring the competitive binding of 8-BODIPY and darapladib with Lp-PLA2. The assay buffer (100 mM Tris pH 7.2, 1 mM

EGTA) containing 15 nM recombinant Lp-PLA2 were incubated with 10 nM **8-BODIPY** for 30 minutes followed by 30 minute-incubation of various concentrations (0.4-100 nM) of darapladib at 25 ℃, and conversely the enzyme was incubated with various concentrations of darapladib followed by addition of 10 nM **8-BODIPY**. After that, the fluorescence polarization (FP) was determined using a BODIPY FP filter set and a BODIPY dichroic mirror (excitation = 485 nm, emission = 528 nm).

Fluorescence imaging of 8-BODIPY in living PC-3 cells. PC-3 cells were seeded on glass bottom culture dishes (NEST Cat. No. 801001). After 24 hours, the cells were first washed with Phosphate Buffered Saline (PBS) 3 times and incubated with 1 μM ER-Tracker Red (Beyotime, C1041) in Hank's Balanced Salt Solution (HBSS, 0.1% DMSO) for 30 minutes at 37 °C. After that the cells were washed with PBS 3 times and incubated with 1 μM **8-BODIPY** and 5 μg/mL Hoechst 33342 in PBS (0.1% DMSO at final) for 10-30 minutes followed by a confocal laser scanning microscopy.

Competitive binding of 8-BODIPY and darapladib with Lp-PLA2 in living Hela cells. Hela cells were seeded in 96-well plates. After 24 h, cells were washed with PBS 3 times followed by 2.5 μM darapladib or DMSO as a control in PBS for 30 min. Then **8-BODIPY**

was added to each well to a final concentration of 1 μM for 10 min. After that, cells were washed with PBS 3 times and images were taken using an Operetta high content imaging system (PerkinElmer). The fluorescence quantification was carried out by the Columbus image data analysis system (PerkinElmer). The mean fluorescence intensity of cell regions calculated separately by Columbus image data analysis system (PerkinElmer).

Synthetic chemistry. All reagents were purchased from commercial suppliers and used without further drying or purification unless otherwise stated. Dry solvents were obtained commercially and stored under a nitrogen atmosphere with activated molecular sieves (MS4A, graininess). Yields were not optimized.

^{1}H NMR and ^{13}C NMR spectra were recorded on a Bruker AC400, a Bruker AC500 or a Bruker AC600 NMR spectrometer in the deuterated solvent stated. Chemical shifts (δ) of the compounds dissolved by deuterated chloroform, were quoted in parts per million (ppm) and using tetramethylsilane (0 ppm) as an internal reference for ^{1}H NMR spectra and the residual non-deuterated solvent signal (77.16 ppm) as an internal reference for ^{13}C NMR spectra, while the chemical shifts (δ) of the compounds dissolved by deuterated methanol (3.31 ppm for ^{1}H NMR spectra and 49.0 ppm for ^{13}C NMR spectra) and

dimethylsulfoxide (2.50 ppm for ^{1}H NMR spectra and 39.5 ppm for ^{13}C NMR spectra) were recorded by using the residual non-deuterated solvent signal as an internal reference. Data are reported as follows: chemical shift (ppm), multiplicity (indicated as: bs, broad signal; s, singlet; d, doublet; t, triplet; q, quartet; p, quintet, sx, sextet; m, multiplet and combinations thereof), coupling constants (*J*) in Hertz (Hz) and integrated intensity. Low-resolution mass spectra were determined on an Agilent liquid-chromatography mass spectrometer system that consisted of an Agilent 1260 infinity LC coupled to Agilent 6120 Quadrupole mass spectrometer (ESI). High-resolution mass spectra were conducted on a triple TOF 5600+ MS/MS system (AB Sciex, Concord, Ontario, Canada) in the negative or positive ESI mode. The purity of all the tested compounds were determined by HPLC using the same analytical method (Table S2) and all the tested compounds possessed ≥ 95% purity. The representative HPLC traces are included in supporting information. Column chromatography was performed on silica gel (200−300 mesh) or with pre-packed silica cartridges (4-40 g) from Bonna-Agela Technologies Inc. (Tianjin, China) and eluted with a CombiFlash@ Rf 200 from Teledyne Isco, and preparative TLC was performed on

HSGF 254 (0.4 − 0.5 mm thickness; Yantai Jiangyou Company, Yantai, Shangdong, China).

General Procedure A: The corresponding aryl halide (1 mmol), (4-formylphenyl) boronic acid (1 mmol), Na_2CO_3 (2 mmol) and $Pd(PPh_3)_4$ (0.1 mmol) were dissolved in a mixed solvent containing toluene, methanol and water (v/v/v = 2/1/1). Under nitrogen atmosphere the mixture was heated to 80 °C and stirred for 16 h. The reaction was quenched with saturated NH_4Cl aqueous solution and extracted with EA for three times. The combined organic layers were washed by saturated aqueous NaCl solution (×3), dried over $MgSO_4$, filtered, and concentrated under reduced pressure. Purification by column chromatography on silica gel afforded the corresponding aryl formaldehyde.

General Procedure B: The solution of aryl formaldehyde (1 mmol) in dry DCM was added by the corresponding amine (1 mmol) and activated molecular sieves (MS4A, graininess). The mixture was stirred for 16 h at 25 ℃ and concentrated under reduced pressure. The residue was redissolved by methanol and stirred another 30 minutes following the addition of $NaBH_4$ (1 mmol). The reaction was directly purified by column chromatography on silica gel to afford the corresponding amine.

General Procedure C: The solution of **5** (1 mmol) in DMF was successively added by the HATU (1.5 mmol), DIPEA (39 μL, 2 mmol) and corresponding amine (38 mg, 1 mmol). The mixture was stirred for 16 h at 25 ℃. The reaction was quenched with saturated NH_4Cl aqueous solution and extracted with EA for three times. The combined organic layers were washed by saturated aqueous NaCl solution (×3), dried over $MgSO_4$, filtered, and concentrated under reduced pressure. Purification by column chromatography on silica gel afforded the corresponding amide.

(*S*,*E*)-2-(3-oxotetrahydro-1*H*,3*H*-pyrrolo[1,2-c]oxazol-1-ylidene)acetic acid (5). The intermediate **5a** was synthesized based on the route reported in the literature.[42] The ^{1}H NMR and ^{13}C spectral data of colorless oily **5a** that we obtained are identical to the literature.[42] ^{1}H NMR (400 MHz, Chloroform-*d*) δ 5.62 (d, *J* = 2.0 Hz, 1H), 4.90 (ddd, *J* = 8.9, 6.7, 1.7 Hz, 1H), 4.24 – 4.16 (m, 2H), 3.72 – 3.63 (m, 1H), 3.28 (ddd, *J* = 11.3, 8.7, 4.7 Hz, 1H), 2.62 (dtd, *J* = 13.1, 6.8, 3.4 Hz, 1H), 2.16 – 1.99 (m, 2H), 1.64 – 1.53 (m, 1H), 1.05 – 0.97 (m, 2H), 0.04 (s, 9H). ^{13}C NMR (126 MHz, Chloroform-d) δ 166.4, 165.4, 156.8, 95.9, 64.3, 62.6, 46.1, 30.4, 26.3, 17.5, -1.4 (3C). LRMS (ESI, *m/z*):284 $[M+H]^+$.

Finally, the solution of **5a** (100 mg, 0.35 mmol) in THF was added by 1M TBAF in THF (1.4 mL, 1.4 mmol). The mixture was stirred for 16 h at 25 ℃. The reaction was quenched with saturated NH_4Cl aqueous solution and extracted with DCM for three times. The combined organic layers were washed by saturated aqueous NaCl solution (×3), dried over MgSO4, filtered, and concentrated under reduced pressure. Purification by column chromatography on silica gel afforded white solid **5** (yield 100%). ^{1}H NMR (500 MHz, Chloroform-*d*) δ 5.67 (d, *J* = 2.0 Hz, 1H), 4.92 (ddd, *J* = 9.0, 6.6, 2.0 Hz, 1H), 3.70 (dt, *J* = 11.4, 7.9 Hz, 1H), 3.31 (ddd, *J* = 11.3, 8.8, 4.6 Hz, 1H), 2.61 (dtd, *J* = 13.2, 7.0, 3.2 Hz, 1H), 2.19 – 2.03 (m, 2H), 1.63 (dq, *J* = 12.7, 9.4 Hz, 1H). ^{13}C NMR (126 MHz, Chloroform-*d*) δ 171.9, 168.0, 156.5, 95.3, 64.5, 46.1, 30.4, 26.4. HRMS (ESI): *m/z* [M-H]$^-$ calculated for $C_8H_8NO_4$, 182.0459; found, 182.0453.

***N*^{1},*N*^{1}-diethyl-*N*^{2}-((4'-(trifluoromethyl)-[1,1'-biphenyl]-4-yl)methyl)ethane-1,2-diamine (6).** ^{1}H NMR (500 MHz, Chloroform-*d*) δ 7.68 (s, 4H), 7.60 – 7.54 (m, 2H), 7.43 (d, *J* = 7.9 Hz, 2H), 3.87 (s, 2H), 2.73 (t, *J* = 6.2 Hz, 2H), 2.62 (t, *J* = 6.2 Hz, 2H), 2.55 (q, *J* = 7.1 Hz, 4H), 1.03 (t, *J* = 7.1 Hz, 6H). ^{13}C NMR (126 MHz, Chloroform-*d*) δ 144.6, 140.7, 138.4, 129.3 (d, *J* = 32.4 Hz), 128.9 (2C), 127.4 (2C), 127.3 (2C), 125.8 (q, *J* = 3.8 Hz, 2C),

124.4 (d, *J* = 271.8 Hz), 53.6, 52.6, 47.1 (2C), 46.8, 11.7 (2C). HRMS (ESI): *m/z* $[M+H]^+$ calculated for $C_{20}H_{26}F_3N_2$, 351.2043; found, 351.2043.

(*S*,*E*)-*N*-(2-(diethylamino)ethyl)-2-(3-oxotetrahydro-1*H*,3*H*-pyrrolo[1,2-c]oxazol-1-ylidene)-*N*-((4'-(trifluoromethyl)-[1,1'-biphenyl]-4-yl)methyl)acetamide (7). Starting with **5** (20 mg, 0.11 mmol) and **6** (38 mg, 0.11 mmol), the white solid **7** was obtained according to the General Procedure C (yield 84%). ^{1}H NMR (400 MHz, Chloroform-*d*) δ 7.67 (t, *J* = 7.0 Hz, 4H), 7.58 (d, *J* = 8.0 Hz, 2H), 7.28 (d, *J* = 8.2 Hz, 2H), 6.00 (d, *J* = 1.9 Hz, 1H), 4.98 (ddd, *J* = 9.0, 6.7, 1.9 Hz, 1H), 4.70 (s, 2H), 3.82 (dt, *J* = 15.0, 5.6 Hz, 1H), 3.75 – 3.62 (m, 2H), 3.34 – 3.16 (m, 6H), 2.84 – 2.67 (m, 1H), 2.60 (dq, *J* = 12.1, 5.7 Hz, 1H), 2.16 – 2.05 (m, 2H), 1.65 (dq, *J* = 12.6, 9.4 Hz, 1H), 1.33 (t, *J* = 7.2 Hz, 6H). ^{13}C NMR (126 MHz, Chloroform-*d*) δ 169.5, 166.9, 156.5, 143.9, 139.9, 135.5, 129.8 (d, *J* = 32.3 Hz), 128.2 (2C), 127.50 (2C), 127.47 (2C), 125.9 (q, *J* = 3.8 Hz), 124.3 (d, *J* = 271.9 Hz), 93.6, 64.6, 53.4, 52.9, 48.4 (2C), 46.1, 44.4, 30.8, 26.3, 9.4 (2C). HRMS (ESI): *m/z* $[M+H]^+$ calculated for $C_{28}H_{33}F_3N_3O_3$, 516.2469; found, 516.2472.

(*S*,*E*)-*N*-(2-(diethylamino)ethyl)-2-(3-oxotetrahydro-1*H*,3*H*-pyrrolo[1,2-c]oxazol-1-ylidene)-*N*-((2'-(2,2,2-trifluoroethoxy)-4'-(trifluoromethyl)-[1,1'-biphenyl]-4-

yl)methyl)acetamide (8). 6a was synthesized following the route reported previously.[58] ^{1}H NMR (400 MHz, Chloroform-*d*) δ 7.72 (d, *J* = 8.2 Hz, 1H), 7.25-7.20 (m, 1H), 7.13 (s, 1H), 4.46 (q, *J* = 7.9 Hz, 2H). ^{13}C NMR (126 MHz, Chloroform-*d*) δ 154.5, 134.7, 131.3 (q, *J* = 33.3 Hz), 123.5 (q, *J* = 273.3.3 Hz), 123.0 (q, *J* = 278.5 Hz), 120.9 (q, *J* = 3.8 Hz), 117.3, 111.5 (q, *J* = 3.8 Hz), 67.3 (q, *J* = 36.6 Hz).

Starting with **6a** (583 mg, 1.81 mmol) and (4-formylphenyl)boronic acid (272 mg, 1.81 mmol), **7a** was obtained as a white solid by using the General Procedure A (81%). ^{1}H NMR (400 MHz, Chloroform-*d*) δ 10.08 (s, 1H), 8.01-7.93 (m, 2H), 7.69 (d, *J* = 8.2 Hz, 2H), 7.53 (d, *J* = 7.9 Hz, 1H), 7.49-7.41 (m, 1H), 7.20 (s, 1H), 4.38 (q, *J* = 7.9 Hz, 2H). ^{13}C NMR (126 MHz, Chloroform-*d*) δ 192.0, 154.4, 142.4, 135.8, 134.0, 131.9 (q, *J* = 32.9 Hz), 131.9, 130.2 (2C), 129.7 (2C), 123.7 (q, *J* = 272.4 Hz), 123.1 (q, *J* = 278.2 Hz), 120.0 (q, *J* = 3.8 Hz), 110.3 (q, *J* = 3.4 Hz), 66.5 (q, *J* = 36.1 Hz). LRMS (ESI, *m/z*):349 $[M+H]^{+}$.

According to the General Procedure B, the colorless oily **8a** was obtained from **7a** (500 mg, 1.44 mmol) and *N*^{1},*N*^{1}-diethylethane-1,2-diamine (202 μL, 1.44 mmol) (yield 73%). ^{1}H NMR (400 MHz, Chloroform-*d*) δ 7.49 (d, *J* = 8.2 Hz, 3H), 7.44-7.38 (m, 3H), 7.19 (s, 1H), 4.30 (q, *J* = 8.0 Hz, 2H), 3.87 (s, 2H), 2.73 (t, *J* = 6.1 Hz, 2H), 2.61 (t, *J* = 6.1

Hz, 2H), 2.53 (q, *J* = 7.1 Hz, 4H), 1.02 (t, *J* = 7.1 Hz, 6H). ^{13}C NMR (126 MHz, Chloroform-*d*) δ 154.4, 137.2, 135.7, 134.9, 131.8 (2C), 130.9 (q, *J* = 32.9 Hz), 129.7 (2C), 128.9, 123.7 (q, *J* = 272.3 Hz), 123.1 (q, *J* = 278.3 Hz), 120.0 (d, *J* = 3.8 Hz), 110.8 (d, *J* = 3.8 Hz), 66.6 (q, *J* = 36.0 Hz), 52.7, 51.3, 46.8 (2C), 44.2, 9.9 (2C). LRMS (ESI, *m/z*):449 $[M+H]^+$.

Starting with **5** (20 mg, 0.11 mmol) and **8a** (49 mg, 0.11 mmol), the white solid **8** was obtained based on the General Procedure C (82%). ^{1}H NMR (500 MHz, Chloroform-*d*) δ 7.52 (d, *J* = 7.9 Hz, 2H), 7.46 (d, *J* = 8.1 Hz, 1H), 7.40 (d, *J* = 8.0 Hz, 1H), 7.26 (d, *J* = 8.0 Hz, 2H), 7.18 (s, 1H), 6.02 (d, *J* = 2.0 Hz, 1H), 4.99 (ddd, *J* = 9.1, 6.7, 1.9 Hz, 1H), 4.70 (s, 2H), 4.35 (q, *J* = 8.0 Hz, 2H), 3.85 (dt, *J* = 12.3, 6.0 Hz, 1H), 3.79 – 3.70 (m, 1H), 3.65 (dt, *J* = 11.1, 7.9 Hz, 1H), 3.31 – 3.16 (m, 6H), 2.83 (q, *J* = 7.3 Hz, 1H), 2.62 (dq, *J* = 12.2, 5.8 Hz, 1H), 2.14 – 2.05 (m, 2H), 1.64 (dq, *J* = 12.8, 9.4 Hz, 1H), 1.32 (t, *J* = 7.3 Hz, 6H). ^{13}C NMR (126 MHz, Chloroform-*d*) δ 168.8, 166.5, 156.6, 154.3, 136.2, 135.5, 134.5, 131.9, 131.0, 130.2 (2C), 126.8 (2C), 123.7 (d, *J* = 272.5 Hz), 123.2 (d, *J* = 278.4 Hz), 120.0 (d, *J* = 3.9 Hz), 110.5, 93.7, 66.5 (d, *J* = 36.1 Hz), 64.6, 52.8, 52.3, 48.1 (2C), 46.0,

43.8, 30.7, 26.2, 9.2 (2C). HRMS (ESI): *m/z* $[M+H]^+$ calculated for $C_{30}H_{34}F_6N_3O_4$, 614.2448; found, 614.2448.

(*S*,*E*)-*N*-((2'-(benzyloxy)-4'-(trifluoromethyl)-[1,1'-biphenyl]-4-yl)methyl)-*N*-(2-(diethylamino)ethyl)-2-(3-oxotetrahydro-1*H*,3*H*-pyrrolo[1,2-c]oxazol-1-ylidene)acetamide (9). The solution of 2-bromo-5-(trifluoromethyl)phenol (500 mg, 2.08 mmol) in DMF was added by (bromomethyl)benzene (249 μL, 2.08 mmol), K_2CO_3 (374 mg, 2.71 mmol) and KI (17 mg, 0.104 mmol). The mixture was stirred for 3 hours at 120 °C. The reaction was quenched with saturated NH_4Cl aqueous solution and extracted with EA for three times. The combined organic layers were washed by saturated aqueous NaCl solution (×3), dried over $MgSO_4$, filtered, and concentrated under reduced pressure. Purification by column chromatography on silica gel afforded the colorless oily **6b** (yield 76%). ^{1}H NMR (400 MHz, Chloroform-*d*) δ 7.71 (d, *J* = 8.1 Hz, 1H), 7.52 (d, *J* = 7.3 Hz, 2H), 7.45 (t, *J* = 7.3 Hz, 2H), 7.38 (t, *J* = 7.2 Hz, 1H), 7.19 (s, 1H), 7.15 (d, *J* = 8.2 Hz, 1H), 5.21 (s, 2H). ^{13}C NMR (126 MHz, Chloroform-*d*) δ 155.5, 135.8, 134.0, 131.0 (q, *J* = 32.7 Hz), 128.8 (2C), 128.4, 127.3 (2C), 123.8 (q, *J* = 272.2 Hz), 118.9 (q, *J* = 3.9 Hz), 116.7, 110.3 (q, *J* = 3.7 Hz), 71.2.

Starting with **6b** (521 mg, 1.58 mmol) and (4-formylphenyl)boronic acid (237 mg, 1.58 mmol), **7b** was obtained as a white solid by using the General Procedure A (79%). ^{1}H NMR (400 MHz, Chloroform-*d*) δ 10.06 (s, 1H), 7.93 (d, *J* = 8.3 Hz, 2H), 7.73 (d, *J* = 8.2 Hz, 2H), 7.47 (d, *J* = 7.9 Hz, 1H), 7.41-7.30 (m, 7H), 5.14 (s, 2H). ^{13}C NMR (126 MHz, Chloroform-*d*) δ 192.0, 155.8, 143.5, 136.0, 135.5, 133.4, 131.7 (q, *J* = 32.5 Hz), 131.3, 130.3 (2C), 129.5 (2C), 128.7 (2C), 128.2, 127.1 (2C), 124.0 (q, *J* = 272.3 Hz), 118.2 (q, *J* = 3.8 Hz), 109.9 (q, *J* = 3.3 Hz), 70.8. LRMS (ESI, *m/z*):357 [M+H]$^{+}$.

According to the General Procedure B, the colorless oily **8b** was obtained from **7b** (500 mg, 1.40 mmol) and *N*^{1},*N*^{1}-diethylethane-1,2-diamine (197 μL, 1.40 mmol) (yield 83%). ^{1}H NMR (400 MHz, Chloroform-*d*) δ 7.53 (d, *J* = 7.9 Hz, 2H), 7.44 (d, *J* = 7.8 Hz, 1H), 7.37 (d, *J* = 7.9 Hz, 2H), 7.35-7.23 (m, 7H), 5.11 (s, 2H), 3.85 (s, 2H), 2.72 (t, *J* = 6.1 Hz, 2H), 2.59 (t, *J* = 6.1 Hz, 2H), 2.51 (q, *J* = 7.1 Hz, 4H), 1.00 (t, *J* = 7.1 Hz, 6H). ^{13}C NMR (126 MHz, Chloroform-*d*) δ 155.7, 137.0, 136.2, 135.2, 134.1, 131.2, 130.7 (q, *J* = 32.5 Hz), 129.9 (2C), 129.0, 128.6 (2C), 128.0(2C), 127.0 (2C), 124.0 (q, *J* = 272.3 Hz), 118.0 (d, *J* = 3.8 Hz), 109.8 (d, *J* = 3.6 Hz), 70.7, 52.4, 50.5, 46.7 (2C), 43.6, 9.6 (2C). LRMS (ESI, *m/z*):457 [M+H]$^{+}$.

Starting with **5** (20 mg, 0.11 mmol) and **8b** (50 mg, 0.11 mmol), the white solid **9** was obtained based on the General Procedure C (80%). ^{1}H NMR (400 MHz, Chloroform-*d*) δ 7.56 (d, *J* = 8.1 Hz, 2H), 7.42 (d, *J* = 7.9 Hz, 1H), 7.38 – 7.29 (m, 6H), 7.26 – 7.20 (m, 3H), 6.04 (d, *J* = 2.0 Hz, 1H), 5.11 (s, 2H), 4.99 (ddd, *J* = 9.0, 6.7, 1.9 Hz, 1H), 4.69 (s, 2H), 3.83 – 3.63 (m, 3H), 3.35 – 3.10 (m, 6H), 2.60 (dq, *J* = 12.1, 5.7 Hz, 1H), 2.11 (dq, *J* = 9.3, 7.1 Hz, 2H), 1.65 (dq, *J* = 12.6, 9.2 Hz, 2H), 1.30 (t, *J* = 7.2 Hz, 6H). ^{13}C NMR (126 MHz, Chloroform-*d*) δ 169.3, 166.9, 156.5, 155.8, 137.5, 136.3, 134.7, 133.9, 131.3, 131.1 (d, *J* = 32.8 Hz), 130.5 (2C), 128.8 (2C), 128.2, 127.2 (2C), 126.6 (2C), 124.1 (d, *J* = 272.5 Hz), 118.3 (d, *J* = 4.1 Hz), 110.0, 93.7, 70.9, 64.6, 53.1, 48.4 (2C), 46.1, 44.5, 30.8, 29.8, 26.3, 9.6 (2C). HRMS (ESI): *m/z* $[M+H]^+$ calculated for $C_{35}H_{39}F_3N_3O_4$, 622.2887; found, 622.2900.

(*S*,*E*)-3-(5,5-difluoro-7,9-dimethyl-5H-4l4,5l4-dipyrrolo[1,2-c:2',1'-f][1,3,2]diazaborinin-3-yl)-*N*-(5-(ethyl(2-(2-(3-oxotetrahydro-1*H*,3*H*-pyrrolo[1,2-c]oxazol-1-ylidene)-*N*-((2'-(2,2,2-trifluoroethoxy)-4'-(trifluoromethyl)-[1,1'-biphenyl]-4-yl)methyl)acetamido)ethyl)amino)pentyl)propanamide (8-BODIPY). The solution of benzyl (2-hydroxyethyl)carbamate (2 g, 10.25 mmol) and DMAP (250 mg, 2.05 mmol) in

DCM was cooled in an ice bath. Then, TsCl (2.15 g, 11.28 mmol) and Et_3N (1.56 mL, 11.28 mmol) in DCM were successively added to this solution. After dropwise addition, the mixture was warmed to 25 ℃ and stirred for 5 hours. The reaction was quenched with saturated NH_4Cl aqueous solution and extracted with DCM for three times. The combined organic layers were washed by saturated aqueous NaCl solution (×3), dried over $MgSO_4$, filtered, and concentrated under reduced pressure. Purification by column chromatography on silica gel afforded white solid **10** (yield 91%). ^{1}H NMR (400 MHz, Chloroform-*d*) δ 7.76 (d, *J* = 8.2 Hz, 2H), 7.40-7.27 (m, 7H), 5.21 (s, 1H), 5.05 (s, 2H), 4.08 (t, *J* = 5.0 Hz, 2H), 3.43 (q, *J* = 5.4 Hz, 2H), 2.42 (s, 3H). ^{13}C NMR (126 MHz, Chloroform-*d*) δ 156.2, 144.9, 136.2, 132.4, 129.8 (2C), 128.3 (2C), 127.9, 127.8 (2C), 127.7 (2C), 68.9, 66.5, 39.9, 21.4. LRMS (ESI, *m/z*):350 $[M+H]^+$.

The solution of **10** (3.26 g, 9.34 mmol) in acetonitrile was added by N-Boc-cadaverine (1.45 g, 7.18 mmol) and K_2CO_3 (2.6 g, 18.68 mmol) and the mixture was stirred for 16 h at 50 °C. Then, the mixture was filtered and the filtrate was directly purified by column chromatography on silica gel to afford colorless oily **11** (yield 51%). ^{1}H NMR (500 MHz, DMSO-d_6) δ 7.35 (d, *J* = 6.1 Hz, 4H), 7.30 (td, *J* = 6.0, 2.4 Hz, 1H), 7.18 (t, *J* = 5.7 Hz,

1H), 6.74 (t, *J* = 5.9 Hz, 1H), 5.01 (s, 2H), 3.09 (q, *J* = 6.3 Hz, 2H), 2.90 (q, *J* = 6.6 Hz, 4H), 2.56 (t, *J* = 6.5 Hz, 2H), 2.46 (t, *J* = 7.1 Hz, 2H), 1.37 (s, 11H), 1.25 (q, *J* = 6.8, 5.4 Hz, 2H). ^{13}C NMR (126 MHz, DMSO-d_6) δ 156.2, 155.6, 137.3, 128.3 (2C), 127.7 (3C), 77.3, 65.2, 49.0, 48.9, 40.4, 29.5, 29.2, 28.3 (3C), 24.1. LRMS (ESI, *m/z*):380 $[M+H]^+$.

11 (1.39 g, 3.67 mmol) and DIPEA (1.28 mL, 7.34 mmol) was dissolved in DMF and added by iodoethane (441 μL, 5.51 mmol). The mixture was stirred for 16 h at 25 ℃. The reaction was quenched with saturated NH_4Cl aqueous solution and extracted with EA for three times. The combined organic layers were washed by saturated aqueous NaCl solution (×3), dried over $MgSO_4$, filtered, and concentrated under reduced pressure. Purification by column chromatography on silica gel afforded colorless oily **12** (yield 68%).^{1}H NMR (600 MHz, DMSO-d_6) δ 7.54 (t, *J* = 5.7 Hz, 1H), 7.36 (d, *J* = 7.2 Hz, 4H), 7.31 (td, *J* = 6.5, 2.8 Hz, 1H), 6.80 (t, *J* = 5.8 Hz, 1H), 5.04 (s, 2H), 3.37 (q, *J* = 6.3 Hz, 2H), 3.07 (q, *J* = 7.2, 6.6 Hz, 4H), 2.96 (d, *J* = 8.1 Hz, 2H), 2.90 (q, *J* = 6.7 Hz, 2H), 1.60 (p, *J* = 8.2, 7.7 Hz, 2H), 1.36 (s, 11H), 1.24 (t, *J* = 9.1 Hz, 2H), 1.18 (t, *J* = 7.2 Hz, 3H). ^{13}C NMR (151 MHz, DMSO-d_6) δ 156.2, 155.7, 136.9, 128.4 (2C), 127.9, 127.8 (2C),

77.4, 65.7, 51.6, 50.4, 47.2, 40.0, 35.5, 29.0, 28.3 (3C), 23.4, 22.7, 8.6. LRMS (ESI, *m/z*):408 $[M+H]^+$.

The air of the solution **12** (1.02 g, 2.50 mmol) in methanol was exchanged with nitrogen and then add Pd/C (100 mg) to this solution. After the nitrogen was further exchanged with hydrogen, the mixture was stirred for 16 h at 25 ℃. The mixture was filtered and the filtrate was evaporated to obtain colorless oily **13** (93%). ^{1}H NMR (400 MHz, Methanol-*d4*) δ 3.07-2.96 (m, 4H), 2.75 (t, *J* = 6.2 Hz, 2H), 2.67 (q, *J* = 7.1 Hz, 2H), 2.61-2.52 (m, 2H), 1.57-1.47 (m, 4H), 1.43 (s, 9H), 1.35-1.32 (d, *J* = 6.7 Hz, 2H), 1.08 (t, *J* = 7.1 Hz, 3H). LRMS (ESI, *m/z*):274 $[M+H]^+$.

According to the General Procedure B, the colorless oily **14** was obtained from **13** (393 mg, 1.44 mmol) and **7a** (500 mg, 1.44 mmol) (yield 85%). ^{1}H NMR (400 MHz, Chloroform-*d*) δ 7.57-7.44 (m, 5H), 7.41 (d, *J* = 8.0 Hz, 1H), 7.18 (s, 1H), 4.34 (q, *J* = 8.0 Hz, 2H), 4.03 (s, 2H), 3.15-2.97 (m, 6H), 2.96-2.90 (m, 2H), 2.81 (t, *J* = 7.6 Hz, 2H), 1.74-1.62 (m, 2H), 1.50 (dt, *J* = 14.5, 7.0 Hz, 2H), 1.43 (s, 9H), 1.37-1.28 (m, 5H). ^{13}C NMR (126 MHz, Chloroform-*d*) δ 156.3, 154.4, 136.3, 135.4, 134.8, 131.9, 131.2 (d, *J* = 32.8 Hz), 129.9 (2C), 129.2 (2C), 123.7 (d, *J* = 272.4 Hz), 123.2 (d, *J* = 278.2 Hz), 120.1 (d, *J*

= 3.6 Hz), 110.7 (d, *J* = 3.4 Hz), 79.3, 66.7 (q, *J* = 35.9 Hz), 52.6, 47.4, 43.6, 40.1, 29.8, 29.7, 28.5 (3C), 24.1, 24.0, 22.8, 9.3. LRMS (ESI, *m/z*):606 $[M+H]^+$.

Starting with **5** (20 mg, 0.11 mmol) and **14** (59 mg, 0.11 mmol), the colorless oily **15** was obtained based on the General Procedure C (65%). ^{1}H NMR (400 MHz, Chloroform-*d*) δ 7.53 (d, *J* = 8.2 Hz, 2H), 7.49 (d, *J* = 8.0 Hz, 1H), 7.42 (d, *J* = 7.8 Hz, 1H), 7.28 (d, *J* = 8.2 Hz, 2H), 7.18 (s, 1H), 6.06-6.01 (m, 1H), 5.04-4.97 (m, 1H), 4.72 (s, 2H), 4.36 (q, *J* = 8.0 Hz, 2H), 3.89-3.62 (m, 3H), 3.35-3.26 (m, 1H), 3.21-2.82 (m, 8H), 2.67-2.59 (m, 1H), 2.17-2.06 (m, 2H), 1.77-1.69 (m, 2H), 1.64 (td, *J* = 9.6, 2.9 Hz, 1H), 1.52 (dt, *J* = 14.2, 7.1 Hz, 2H), 1.43 (s, 9H), 1.33-1.28 (m, 5H). ^{13}C NMR (126 MHz, Chloroform-*d*) δ 166.5, 164.9, 156.9, 156.2, 154.4, 137.7, 136.5, 135.9, 134.7, 131.9, 131.1 (q, *J* = 33.0 Hz), 130.1 (2C), 129.7, 127.9, 126.7 (2C), 123.7 (d, *J* = 272.3 Hz), 123.1 (d, *J* = 278.3 Hz), 120.0 (d, *J* = 3.6 Hz), 110.6 (d, *J* = 3.4 Hz), 94.4, 79.2, 66.6 (q, *J* = 35.9 Hz), 64.5, 52.5, 49.7, 49.3, 47.5, 46.0, 40.0, 30.8, 29.8, 29.6, 28.5 (3C), 26.3, 24.1, 9.4. LRMS (ESI, *m/z*):771 $[M+H]^+$.

15 was dissolved in a mixed solvent containing DCM and TFA (v/v = 5:1). The mixture was stirred for 16 h at 25 ℃. The reaction was quenched with $NaHCO_3$ aqueous solution

and extracted with DCM for three times. The combined organic layers were washed by saturated aqueous NaCl solution (×3), dried over $MgSO_4$, filtered, and concentrated under reduced pressure. Purification by column chromatography on silica gel afforded colorless oily **16** (yield 77%). ^{1}H NMR (400 MHz, Methanol-*d4*) δ 7.62-7.51 (m, 3H), 7.47-7.41 (m, 2H), 7.35 (t, *J* = 7.7 Hz, 2H), 6.26-6.22 (m, 1H), 5.10-5.02 (m, 1H), 4.81 (s, 2H), 4.64-4.61 (m, 2H), 3.84-3.76 (m, 1H), 3.67-3.55 (m, 2H), 3.30-3.08 (m, 7H), 2.97-2.89 (m, 2H), 2.64-2.58 (m, 1H), 2.16-2.08 (m, 2H), 1.69-1.66 (m, 1H), 1.62-1.59 (m, 2H), 1.49-1.42 (m, 2H), 1.39-1.37 (m, 5H). HRMS (ESI): *m/z* $[M+H]^+$ calculated for $C_{33}H_{41}F_6N_4O_4$, 671.3027; found, 671.3011.

Starting with **16** (20 mg, 0.030 mmol) and **17a** (9 mg, 0.030 mmol), the orange red solid **8-BIDOPY** was obtained based on the General Procedure C (85%). ^{1}H NMR (500 MHz, Chloroform-*d*) δ 7.48 (ddd, *J* = 14.5, 7.4, 5.3 Hz, 3H), 7.42 – 7.37 (m, 1H), 7.29 (d, *J* = 7.9 Hz, 1H), 7.23 (d, *J* = 7.8 Hz, 1H), 7.18 (s, 1H), 7.09 (d, *J* = 16.3 Hz, 1H), 6.87 (dd, *J* = 7.9, 3.6 Hz, 1H), 6.27 (d, *J* = 3.1 Hz, 1H), 6.14 – 5.96 (m, 3H), 5.29 (d, *J* = 1.8 Hz, 1H), 5.08 – 4.97 (m, 1H), 4.79 – 4.61 (m, 2H), 4.35 (q, *J* = 8.0 Hz, 2H), 3.70 – 3.48 (m, 2H), 3.36 (t, *J* = 7.1 Hz, 1H), 3.31 – 3.22 (m, 3H), 3.22 – 3.15 (m, 2H), 2.90 – 2.83 (m,

1H), 2.81 – 2.73 (m, 1H), 2.71 – 2.57 (m, 4H), 2.56 – 2.50 (m, 4H), 2.48 (q, *J* = 7.1 Hz, 1H), 2.37 (t, *J* = 7.4 Hz, 1H), 2.23 (s, 3H), 2.13 – 2.00 (m, 2H), 1.62 (dq, *J* = 12.5, 9.4 Hz, 1H), 1.54 – 1.48 (m, 1H), 1.45 (q, *J* = 7.5 Hz, 2H), 1.38 (p, *J* = 7.9 Hz, 1H), 1.14 – 0.95 (m, 3H). ^{13}C NMR (126 MHz, Chloroform-*d*) δ 172.0, 165.7, 163.9, 160.2, 157.8, 157.2, 154.4, 144.1, 137.7, 136.3, 135.3, 135.0, 133.5, 131.8, 131.0 (d, *J* = 33.3 Hz), 130.1 (2C), 128.5 (2C), 127.8, 124.0, 123.7 (d, *J* = 273.9 Hz), 123.1 (d, *J* = 278.4 Hz), 120.5, 120.0, 117.5, 110.8, 94.9, 66.6 (q, *J* = 35.7 Hz), 64.5, 53.8, 52.6, 49.2, 48.1, 46.0, 39.5, 35.9, 30.8, 29.6, 29.08, 27.0, 26.3, 25.0, 24.7, 15.0, 11.9, 11.3. HRMS (ESI): *m/z* $[M+H]^+$ calculated for $C_{47}H_{54}[11B]F_8N_6O_5$, 945.4116; found, 945.4132

(*S,E*)-2-(6-(diethylamino)-3-(diethyliminio)-3H-xanthen-9-yl)-5-(*N*-(5-(ethyl(2-(2-(3-oxotetrahydro-1*H*,3*H*-pyrrolo[1,2-c]oxazol-1-ylidene)-*N*-((2'-(2,2,2-trifluoroethoxy)-4'-(trifluoromethyl)-[1,1'-biphenyl]-4-yl)methyl)acetamido)ethyl)amino)pentyl)sulfamoyl)benzenesulfonate (8-RH). According to the synthesized route of **12**, the bright red solid **8-RH** was obatained from **16** (20 mg, 0.030 mmol) and **17b** (18 mg, 0.030 mmol) (yield 81%). ^{1}H NMR (500 MHz, DMSO-d_6) δ 8.4 (d, *J* = 1.8 Hz, 1H), 8.0 – 7.8 (m, 2H), 7.6 – 7.5 (m, 3H), 7.5 – 7.4 (m, 3H), 7.3 (t, *J* =

8.5 Hz, 2H), 7.1 – 6.9 (m, 4H), 6.9 (d, *J* = 2.2 Hz, 2H), 6.3 – 6.2 (m, 1H), 5.0 – 4.9 (m, 3H), 4.8 – 4.6 (m, 2H), 3.7 – 3.6 (m, 8H), 3.5 – 3.4 (m, 1H), 3.4 – 3.4 (m, 2H), 3.2 – 3.2 (m, 1H), 2.9 (q, *J* = 6.9, 5.7 Hz, 2H), 2.5 (dd, *J* = 11.6, 5.2 Hz, 4H), 2.4 – 2.3 (m, 2H), 2.0 – 1.9 (m, 3H), 1.6 (dq, *J* = 12.7, 9.8 Hz, 1H), 1.4 (p, *J* = 6.9, 6.4 Hz, 2H), 1.3 (dt, *J* = 14.4, 8.1 Hz, 2H), 1.3 – 1.2 (m, 2H), 1.2 (t, *J* = 7.1 Hz, 12H), 0.9 (t, *J* = 7.0 Hz, 3H). ^{13}C NMR (126 MHz, DMSO-d_6) δ 165.0, 162.7, 157.5, 157.1 (2C), 156.5, 155.0 (2C), 153.9, 148.1, 141.7, 138.2, 134.6, 133.9, 132.9, 132.7 (2C), 131.6, 130.5, 129.4, 129.3 (d, *J* = 32.4 Hz), 129.2 (2C), 127.3 (2C), 126.47 (2C), 125.7, 123.9 (d, *J* = 272.5 Hz), 123.8 (d, *J* = 277.8 Hz), 119.1 (d, *J* = 4.1 Hz), 113.6 (2C), 113.5 (2C), 110.4, 95.4, 65.1 (q, *J* = 35.0 Hz), 63.7, 63.7, 54.9, 53.0, 48.2, 47.3, 45.6, 45.3 (4C), 42.6, 30.2, 30.1, 29.1, 29.0, 25.7, 23.9, 12.4 (4C). HRMS (ESI): *m/z* $[M+H]^+$ calculated for $C_{60}H_{69}F_6N_6O_{10}S_2$, 1211.4415; found, 1211.4409.

ASSOCIATED CONTENT

Supporting Information

The supporting information is available free of charge http://pubs.acs.org.

The determination of the reactivity of fragment **5** with glutathione (GSH); Lp-PLA2 protein expression and purification; the evaluation of the time-dependent inhibition of compounds **7** and **8** against Lp-PLA2; mass-spectroscopic analysis of Lp-PLA2 incubated with compound **7**; Figures S1-S12, Tables S1-S12, and Representative HPLC traces. (PDF)

Molecular formula strings (CSV)

AUTHOR INFORMATION

Corresponding Authors

[*] Jianhua Shen, jhshen@simm.ac.cn

and Yechun Xu, ycxu@simm.ac.cn

Author Contributions

[#] Fubao Huang and Hangchen Hu contributed equally to this work.

F.H., H.H., K.W., W.X. and Y.L. designed and synthesized the compounds. H.H. designed and carried out the biological assays and determined the crystal structures. J.G. and H.Z. contributed to the mass-spectroscopic analysis of Lp-PLA2 incubated with

covalent fragments. M.L. contributed to determine the crystal structures. H.H., C.P., Y.Z., and R.H. carried out the fluorescence imaging of **8-BODIPY** in living PC-3 cells. Y.X. and J.S. supervised and contributed to the design and interpretation of the data. H.H., F.H. and Y.X. wrote the manuscript with inputs from all authors. All authors approved the final manuscript.

Funding Sources

This work was supported by the National Key R&D Program of China (No. 2016YFA0502301), National Science & Technology Major Project 'Key New Drug Creation and Manufacturing Program' China (Grant No. 2018ZX09711002-006-014) and the National Natural Science Foundation of China (Grant No. 21877122 and Grant No. 81602963).

Notes

The authors declare no competing financial interest.

ACKNOWLEDGMENT

We thank Prof. Ruimin Huang for the help with in-gel fluorescent scanning.

ABBREVIATIONS

NH_4Cl, ammonium chloride; HATU, 1-[bis(dimethylamino)methylene]-1H-1,2,3-triazolo[4,5-b]pyridinium 3-oxide hexafluorophosphate; DCM, dichloromethane; EA, ethyl acetate; TsCl, 4-toluene sulfonyl chloride; DIPEA, *N,N*-diisopropylethylamine; DMF, *N,N*-dimethylformamide; MeCN, acetonitrile; THF, tetrahydrofuran; K_2CO_3, potassium carbonate; Na_2CO_3, sodium carbonate; $NaHCO_3$, sodium bicarbonate; Et_3N, trimethylamine; DMAP, (4-dimethylaminopyridine; min, minute; MeOH, methanol; $NaBH_4$, sodium borohydride; TBAF, tetrabutylammonium fluoride; $MgSO_4$, magnesium sulphate; NaCl, sodium chloride; PPh_3, triphenylphosphine; $Pd(PPh_3)_4$, tetrakis(triphenylphosphine)palladium(0) and TFA, trifluoroacetic acid, HPLC, high performance liquid chromatography.

ANCILLARY INFORMATION

The authors will release the atomic coordinates and experimental data upon article publication.

REFERENCES

(1) Gehringer, M.; Laufer, S. A. Emerging and re-emerging warheads for targeted covalent inhibitors: applications in medicinal chemistry and chemical biology. *J. Med. Chem.* **2019,** 62, 5673-5724.

(2) Lonsdale, R.; Ward, R. A. Structure-based design of targeted covalent inhibitors. *Chem. Soc. Rev.* **2018,** 47, 3816-3830.

(3) Heal, W. P.; Dang, T. H.; Tate, E. W. Activity-based probes: discovering new biology and new drug targets. *Chem. Soc. Rev.* **2011,** 40, 246-257.

(4) Cravatt, B. F.; Wright, A. T.; Kozarich, J. W. Activity-based protein profiling: from enzyme chemistry to proteomic chemistry. *Annu. Rev. Biochem.* **2008,** 77, 383-414.

(5) Martin-Gago, P.; Olsen, C. A. Arylfluorosulfate-based electrophiles for covalent protein labeling: a new addition to the arsenal. *Angew. Chem. Int. Ed.* **2019,** 58, 957-966.

(6) Noe, M. C.; Gilbert, A. M. Targeted covalent enzyme inhibitors. *Annu. Rep. Med. Chem.* **2012,** 47, 413-439.

(7) Niphakis, M. J.; Cravatt, B. F. Enzyme inhibitor discovery by activity-based protein profiling. *Annu. Rev. Biochem.* **2014,** 83, 341-377.

(8) Singh, J.; Petter, R. C.; Baillie, T. A.; Whitty, A. The resurgence of covalent drugs. *Nat. Rev. Drug Discov.* **2011,** 10, 307-317.

(9) Lagoutte, R.; Winssinger, N. Following the lead from nature with covalent inhibitors. *Chimia* **2017,** 71, 703-711.

(10) Pettinger, J.; Le Bihan, Y. V.; Widya, M.; van Montfort, R. L. M.; Jones, K.; Cheeseman, M. D. An irreversible inhibitor of HSP72 that unexpectedly targets lysine-56. *Angew. Chem. Int. Ed.* **2017,** 56, 3536-3540.

(11) Lelais, G.; Epple, R.; Marsilje, T. H.; Long, Y. O.; McNeill, M.; Chen, B.; Lu, W. S.; Anumolu, J.; Badiger, S.; Bursulaya, B.; DiDonato, M.; Fong, R. N.; Juarez, J.; Li, J.; Manuia, M.; Mason, D. E.; Gordon, P.; Groessl, T.; Johnson, K.; Jia, Y.; Kasibhatla, S.; Li, C.; Isbell, J.; Spraggon, G.; Bender, S.; Michellys, P. Y. Discovery of (*R*,*E*)-*N*-(7-chloro-1-(1-[4-(dimethylamino)but-2-enoyl]azepan-3-yl)-1H-benzo[d]imidazol-2-yl)-2-methylisonicotinamide (EGF816), a novel, potent, and WT sparing covalent inhibitor of oncogenic (L858R, ex19del) and resistant (T790M) EGFR mutants for the treatment of EGFR mutant non-small-cell lung cancers. *J. Med. Chem.* **2016,** 59, 6671-6689.

(12) Tan, L.; Wang, J.; Tanizaki, J.; Huang, Z. F.; Aref, A. R.; Rusan, M.; Zhu, S. J.; Zhang, Y. Y.; Ercan, D.; Liao, R. G.; Capelletti, M.; Zhou, W. J.; Hur, W.; Kim, N.; Sim, T.; Gaudet, S.; Barbie, D. A.; Yeh, J. R. J.; Yun, C. H.; Hammerman, P. S.; Mohammadi, M.; Janne, P. A.; Gray, N. S. Development of covalent inhibitors that can overcome resistance to first-generation FGFR kinase inhibitors. *Proc. Natl. Acad. Sci. U. S. A.* **2014,** 111, E4869-E4877.

(13) Kung, A.; Chen, Y. C.; Schimpl, M.; Ni, F.; Zhu, J. F.; Turner, M.; Molina, H.; Overman, R.; Zhang, C. Development of specific, irreversible inhibitors for a receptor tyrosine kinase EphB3. *J. Am. Chem. Soc.* **2016,** 138, 10554-10560.

(14) Chaikuad, A.; Koch, P.; Laufer, S. A.; Knapp, S. The cysteinome of protein kinases as a target in drug development. *Angew. Chem. Int. Ed.* **2018,** 57, 4372-4385.

(15) Huang, F.; Wang, K.; Shen, J. Lipoprotein-associated phospholipase A2: the story continues. *Med. Res. Rev.* **2020,** 40, 79-134.

(16) Donato, L. J.; Meeusen, J. W.; Callanan, H.; Saenger, A. K.; Jaffe, A. S. Advantages of the lipoprotein-associated phospholipase A2 activity assay. *Clin. Biochem.* **2016,** 49, 172-175.

(17) Acharya, N. K.; Levin, E. C.; Clifford, P. M.; Han, M.; Tourtellotte, R.; Chamberlain, D.; Pollaro, M.; Coretti, N. J.; Kosciuk, M. C.; Nagele, E. P.; Demarshall, C.; Freeman, T.; Shi, Y.; Guan, C.; Macphee, C. H.; Wilensky, R. L.; Nagele, R. G. Diabetes and hypercholesterolemia increase blood-brain barrier permeability and brain amyloid deposition: beneficial effects of the LpPLA2 inhibitor darapladib. *J. Alzheimers Dis.* **2013,** 35, 179-198.

(18) Maher-Edwards, G.; De'Ath, J.; Barnett, C.; Lavrov, A.; Lockhart, A. A 24-week study to evaluate the effect of rilapladib on cognition and cerebrospinal fluid biomarkers of Alzheimer's disease. *Alzheimers Dement (N Y)* **2015,** 1, 131-140.

(19) Acharya, N. K.; Qi, X.; Goldwaser, E. L.; Godsey, G. A.; Wu, H.; Kosciuk, M. C.; Freeman, T. A.; Macphee, C. H.; Wilensky, R. L.; Venkataraman, V.; Nagele, R. G. Retinal pathology is associated with increased blood-retina barrier permeability in a diabetic and hypercholesterolaemic pig model: Beneficial effects of the LpPLA2 inhibitor Darapladib. *Diab. Vasc. Dis. Res.* **2017,** 14, 200-213.

(20) Canning, P.; Kenny, B. A.; Prise, V.; Glenn, J.; Sarker, M. H.; Hudson, N.; Brandt, M.; Lopez, F. J.; Gale, D.; Luthert, P. J.; Adamson, P.; Turowski, P.; Stitt, A. W.

Lipoprotein-associated phospholipase A(2) (Lp-PLA(2)) as a therapeutic target to prevent retinal vasopermeability during diabetes. *Proc. Natl. Acad. Sci. U. S. A.* **2016,** 113, 7213-7218.

(21) Staurenghi, G.; Ye, L.; Magee, M. H.; Danis, R. P.; Wurzelmann, J.; Adamson, P.; McLaughlin, M. M. Darapladib, a lipoprotein-associated phospholipase A2 inhibitor, in diabetic macular edema: a 3-month placebo-controlled study. *Ophthalmology* **2015,** 122, 990-996.

(22) O'Donoghue, M. L.; Braunwald, E.; White, H. D.; Steen, D. P.; Lukas, M. A.; Tarka, E.; Steg, P. G.; Hochman, J. S.; Bode, C.; Maggioni, A. P.; Im, K.; Shannon, J. B.; Davies, R. Y.; Murphy, S. A.; Crugnale, S. E.; Wiviott, S. D.; Bonaca, M. P.; Watson, D. F.; Weaver, W. D.; Serruys, P. W.; Cannon, C. P.; Investigators, S.-T. Effect of darapladib on major coronary events after an acute coronary syndrome The SOLID-TIMI 52 Randomized Clinical Trial. *J. Am. Med. Assoc.* **2014,** 312, 1006-1015.

(23) White, H. D.; Held, C.; Stewart, R.; Tarka, E.; Brown, R.; Davies, R. Y.; Budaj, A.; Harrington, R. A.; Steg, P. G.; Ardis-Sino, D.; Armstrong, P. W.; Avezum, A.; Aylward, P. E.; Bryce, A.; Chen, H.; Chen, M. F.; Corbalan, R.; Dalby, A. J.; Danchin, N.; De Winter,

R. J.; Denchev, S.; Diaz, R.; Elisaf, M.; Flather, M. D.; Goudev, A. R.; Granger, C. B.; Grinfeld, L.; Hochman, J. S.; Husted, S.; Kim, H. S.; Koenig, W.; Linhart, A.; Lonn, E.; Lopez-Sendon, J.; Manolis, A. J.; Mohler, E. R.; Nicolau, J. C.; Pais, P.; Parkhomenko, A.; Pedersen, T. R.; Pella, D.; Ramos-Corrales, M. A.; Ruda, M.; Sereg, M.; Siddique, S.; Sinnaeve, P.; Smith, P.; Sritara, P.; Swart, H. P.; Sy, R. G.; Teramoto, T.; Tse, H. F.; Watson, D.; Weaver, W. D.; Weiss, R.; Viigimaa, M.; Vinereanu, D.; Zhu, J. R.; Cannon, C. P.; Wallentin, L.; Investigators, S. Darapladib for preventing ischemic events in stable coronary heart disease. *New. Engl. J. Med.* **2014,** 370, 1702-1711.

(24) Liu, Q.; Huang, F.; Yuan, X.; Wang, K.; Zou, Y.; Shen, J.; Xu, Y. Structure-guided discovery of novel, potent, and orally bioavailable inhibitors of lipoprotein-associated phospholipase A2. *J. Med. Chem.* **2017,** 60, 10231-10244.

(25) Murray, C. W.; Rees, D. C. The rise of fragment-based drug discovery. *Nat. Chem.* **2009,** 1, 187-192.

(26) Hajduk, P. J.; Greer, J. A decade of fragment-based drug design: strategic advances and lessons learned. *Nat. Rev. Drug Discov.* **2007,** 6, 211-219.

(27) Nonoo, R. H.; Armstrong, A.; Mann, D. J. Kinetic template-guided tethering of fragments. *Chem. Med. Chem.* **2012,** 7, 2082-2086.

(28) Jost, C.; Nitsche, C.; Scholz, T.; Roux, L.; Klein, C. D. Promiscuity and selectivity in covalent enzyme inhibition: a systematic study of electrophilic fragments. *J. Med. Chem.* **2014,** 57, 7590-7599.

(29) Kathman, S. G.; Xu, Z.; Statsyuk, A. V. A fragment-based method to discover irreversible covalent inhibitors of cysteine proteases. *J. Med. Chem.* **2014,** 57, 4969-4974.

(30) Craven, G. B.; Affron, D. P.; Allen, C. E.; Matthies, S.; Greener, J. G.; Morgan, R. M. L.; Tate, E. W.; Armstrong, A.; Mann, D. J. High-throughput kinetic analysis for target-directed covalent ligand discovery. *Angew. Chem. Int. Ed.* **2018,** 57, 5257-5261.

(31) Johansson, H.; Isabella Tsai, Y. C.; Fantom, K.; Chung, C. W.; Kumper, S.; Martino, L.; Thomas, D. A.; Eberl, H. C.; Muelbaier, M.; House, D.; Rittinger, K. Fragment-based covalent ligand screening enables rapid discovery of inhibitors for the RBR E3 ubiquitin ligase HOIP. *J. Am. Chem. Soc.* **2019,** 141, 2703-2712.

(32) Resnick, E.; Bradley, A.; Gan, J.; Douangamath, A.; Krojer, T.; Sethi, R.; Geurink, P. P.; Aimon, A.; Amitai, G.; Bellini, D.; Bennett, J.; Fairhead, M.; Fedorov, O.; Gabizon, R.;

Gan, J.; Guo, J.; Plotnikov, A.; Reznik, N.; Ruda, G. F.; Diaz-Saez, L.; Straub, V. M.; Szommer, T.; Velupillai, S.; Zaidman, D.; Zhang, Y.; Coker, A. R.; Dowson, C. G.; Barr, H. M.; Wang, C.; Huber, K. V. M.; Brennan, P. E.; Ovaa, H.; von Delft, F.; London, N. Rapid covalent-probe discovery by electrophile-fragment screening. *J. Am. Chem. Soc.* **2019,** 141, 8951-8968.

(33) Miller, R. M.; Paavilainen, V. O.; Krishnan, S.; Serafimova, I. M.; Taunton, J. Electrophilic fragment-based design of reversible covalent kinase inhibitors. *J. Am. Chem. Soc.* **2013,** 135, 5298-5301.

(34) Lee, C. U.; Grossmann, T. N. Reversible covalent inhibition of a protein target. *Angew. Chem. Int. Ed.* **2012,** 51, 8699-8700.

(35) Barf, T.; Kaptein, A. Irreversible protein kinase inhibitors: balancing the benefits and risks. *J. Med. Chem.* **2012,** 55, 6243-6262.

(36) MacPhee, C. H.; Moores, K. E.; Boyd, H. F.; Dhanak, D.; Ife, R. J.; Leach, C. A.; Leake, D. S.; Milliner, K. J.; Patterson, R. A.; Suckling, K. E.; Tew, D. G.; Hickey, D. M. Lipoprotein-associated phospholipase A2, platelet-activating factor acetylhydrolase,

generates two bioactive products during the oxidation of low-density lipoprotein: use of a novel inhibitor. *Biochem. J.* **1999,** 338 (Pt 2), 479-487.

(37) Nagano, J. M.; Hsu, K. L.; Whitby, L. R.; Niphakis, M. J.; Speers, A. E.; Brown, S. J.; Spicer, T.; Fernandez-Vega, V.; Ferguson, J.; Hodder, P.; Srinivasan, P.; Gonzalez, T. D.; Rosen, H.; Bahnson, B. J.; Cravatt, B. F. Selective inhibitors and tailored activity probes for lipoprotein-associated phospholipase A(2). *Bioorg. Med. Chem. Lett.* **2013,** 23, 839-843.

(38) Thirkettle, J.; Alvarez, E.; Boyd, H.; Brown, M.; Diez, E.; Hueso, J.; Elson, S.; Fulston, M.; Gershater, C.; Morata, M. L.; Perez, P.; Ready, S.; Sanchez-Puelles, J. M.; Sheridan, R.; Stefanska, A.; Warr, S. SB-253514 and analogues; novel inhibitors of lipoprotein-associated phospholipase A2 produced by Pseudomonas fluorescens *DSM 11579*. I. Fermentation of producing strain, isolation and biological activity. *J. Antibiot. (Tokyo)* **2000,** 53, 664-669.

(39) Drawz, S. M.; Bonomo, R. A. Three decades of beta-lactamase inhibitors. *Clin. Microbiol. Rev.* **2010,** 23, 160-201.

(40) Ross, M. K.; Wang, R. Expanding the toolkit for the serine hydrolases. *Chem. Biol.* **2015,** 22, 808-809.

(41) Dockerty, P.; Edens, J. G.; Tol, M. B.; Morales Angeles, D.; Domenech, A.; Liu, Y.; Hirsch, A. K.; Veening, J. W.; Scheffers, D. J.; Witte, M. D. Bicyclic enol cyclocarbamates inhibit penicillin-binding proteins. *Org. Biomol. Chem.* **2017,** 15, 894-910.

(42) Duvall, J. R.; Wu, F.; Snider, B. B. Structure reassignment and synthesis of Jenamidines A1/A2, synthesis of (+)-NP25302, and formal synthesis of SB-311009 analogues. *J. Org. Chem.* **2006,** 71, 8579-8590.

(43) Pinto, I. L.; Boyd, H. F.; Hickey, D. M. Natural product derived inhibitors of lipoprotein associated phospholipase A2, synthesis and activity of analogues of SB-253514. *Bioorg. Med. Chem. Lett.* **2000,** 10, 2015-2017.

(44) Cee, V. J.; Volak, L. P.; Chen, Y.; Bartberger, M. D.; Tegley, C.; Arvedson, T.; McCarter, J.; Tasker, A. S.; Fotsch, C. Systematic study of the glutathione (GSH) reactivity of N-arylacrylamides: 1. effects of aryl substitution. *J. Med. Chem.* **2015,** 58, 9171-9178.

(45) Lonsdale, R.; Burgess, J.; Colclough, N.; Davies, N. L.; Lenz, E. M.; Orton, A. L.; Ward, R. A. Expanding the armory: Predicting and tuning covalent warhead reactivity. *J. Chem. Inf. Model* **2017,** 57, 3124-3137.

(46) Liu, Q. F.; Chen, X. D.; Chen, W. Y.; Yuan, X. J.; Su, H. X.; Shen, J. H.; Xu, Y. C. Structural and thermodynamic characterization of protein-ligand interactions formed between lipoprotein-associated phospholipase A2 and inhibitors. *J. Med. Chem.* **2016,** 59, 5115-5120.

(47) Long, J. Z.; Cravatt, B. F. The metabolic serine hydrolases and their functions in mammalian physiology and disease. *Chem. Rev.* **2011,** 111, 6022-6063.

(48) Tjoelker, L. W.; Wilder, C.; Eberhardt, C.; Stafforini, D. M.; Dietsch, G.; Schimpf, B.; Hooper, S.; Le Trong, H.; Cousens, L. S.; Zimmerman, G. A.; Yamada, Y.; McIntyre, T. M.; Prescott, S. M.; Gray, P. W. Anti-inflammatory properties of a platelet-activating factor acetylhydrolase. *Nature* **1995,** 374, 549-553.

(49) Foulks, J. M.; Marathe, G. K.; Michetti, N.; Stafforini, D. M.; Zimmerman, G. A.; McIntyre, T. M.; Weyrich, A. S. PAF-acetylhydrolase expressed during megakaryocyte differentiation inactivates PAF-like lipids. *Blood* **2009,** 113, 6699-6706.

(50) Guibbal, F.; Benard, S.; Patche, J.; Meneyrol, V.; Couprie, J.; Yong-Sang, J.; Meilhac, O.; Jestin, E. Regioselectivity of thiouracil alkylation: Application to optimization of Darapladib synthesis. *Bioorg. Med. Chem. Lett.* **2018,** 28, 787-792.

(51) Chen, X.; Wang, K.; Xu, W.; Ma, Q.; Chen, M.; Du, L.; Mo, M.; Wang, Y.; Shen, J. Discovery of Potent and Orally Active Lipoprotein-associated phospholipase A2 (Lp-PLA2) inhibitors as a potential Therapy for diabetic macular edema. *J. Med. Chem.* **2016,** 59, 2674-2687.

(52) Wang, Q. S.; Yu, F.; Huang, S.; Sun, B.; Zhang, K. H.; Liu, K.; Wang, Z. J.; Xu, C. Y.; Wang, S. S.; Yang, L. F.; Pan, Q. Y.; Li, L.; Zhou, H.; Cui, Y.; Xu, Q.; Earnest, T.; He, J. H. The macromolecular crystallography beamline of SSRF. *Nucl. Sci. Tech.* **2015,** 26, 12-17.

(53) Minor, W.; Cymborowski, M.; Otwinowski, Z.; Chruszcz, M. HKL-3000: the integration of data reduction and structure solution - from diffraction images to an initial model in minutes. *Acta. Crystallogr. D. Biol. Crystallogr.* **2006,** 62, 859-866.

(54) Mccoy, A. J.; Grosse-Kunstleve, R. W.; Adams, P. D.; Winn, M. D.; Storoni, L. C.; Read, R. J. Phaser crystallographic software. *J. Appl. Crystallogr.* **2007,** 40, 658-674.

(55) Adams, P. D.; Afonine, P. V.; Bunkoczi, G.; Chen, V. B.; Davis, I. W.; Echols, N.; Headd, J. J.; Hung, L. W.; Kapral, G. J.; Grosse-Kunstleve, R. W.; McCoy, A. J.; Moriarty, N. W.; Oeffner, R.; Read, R. J.; Richardson, D. C.; Richardson, J. S.; Terwilliger, T. C.; Zwart, P. H. PHENIX: a comprehensive Python-based system for macromolecular structure solution. *Acta. Crystallogr. D. Biol. Crystallogr.* **2010,** 66, 213-221.

(56) Vagin, A. A.; Steiner, R. A.; Lebedev, A. A.; Potterton, L.; McNicholas, S.; Long, F.; Murshudov, G. N. REFMAC5 dictionary: organization of prior chemical knowledge and guidelines for its use. *Acta. Crystallogr. D. Biol. Crystallogr.* **2004,** 60, 2184-2195.

(57) Emsley, P.; Lohkamp, B.; Scott, W. G.; Cowtan, K. Features and development of Coot. *Acta. Crystallogr. D. Biol. Crystallogr.* **2010,** 66, 486-501.

(58) Lee, S. R.; Bloom, J. W.; Wheeler, S. E.; McNeil, A. J. Accelerating Ni(II) precatalyst initiation using reactive ligands and its impact on chain-growth polymerizations. *Dalton Trans.* **2013,** 42, 4218-4222.

Table of contents graphic

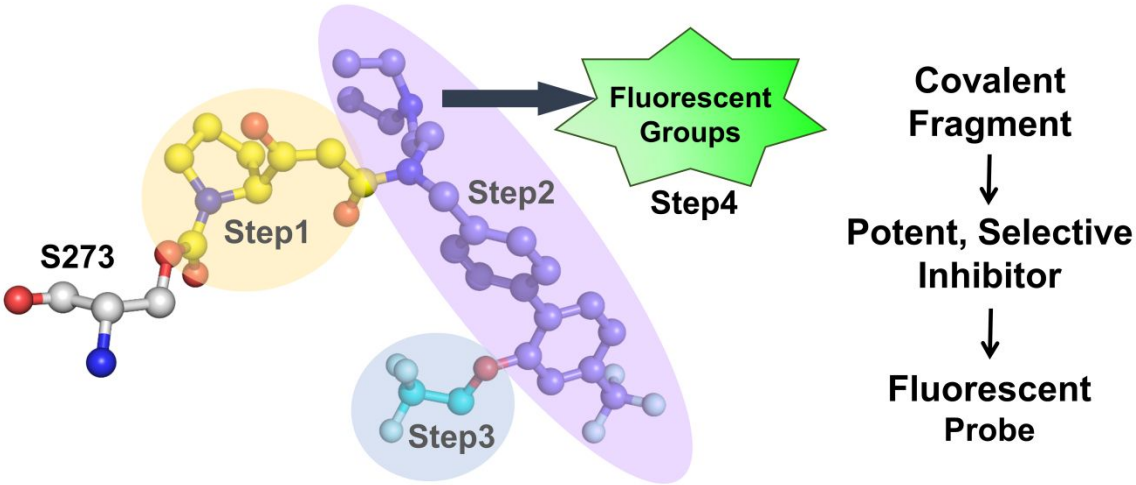

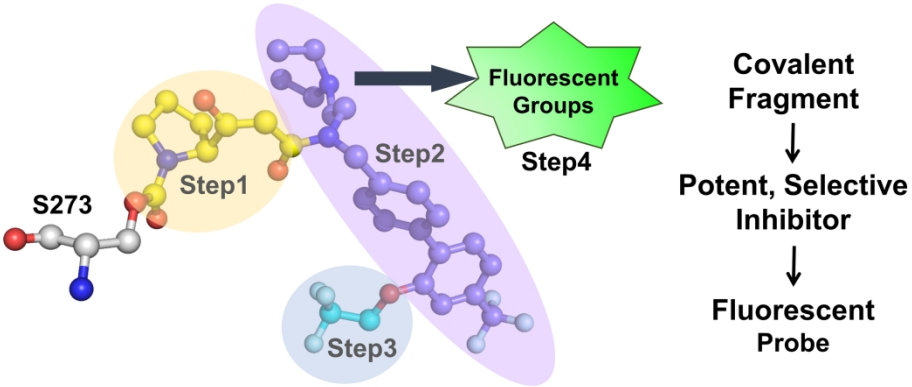

TOC

244x116mm (300 x 300 DPI)

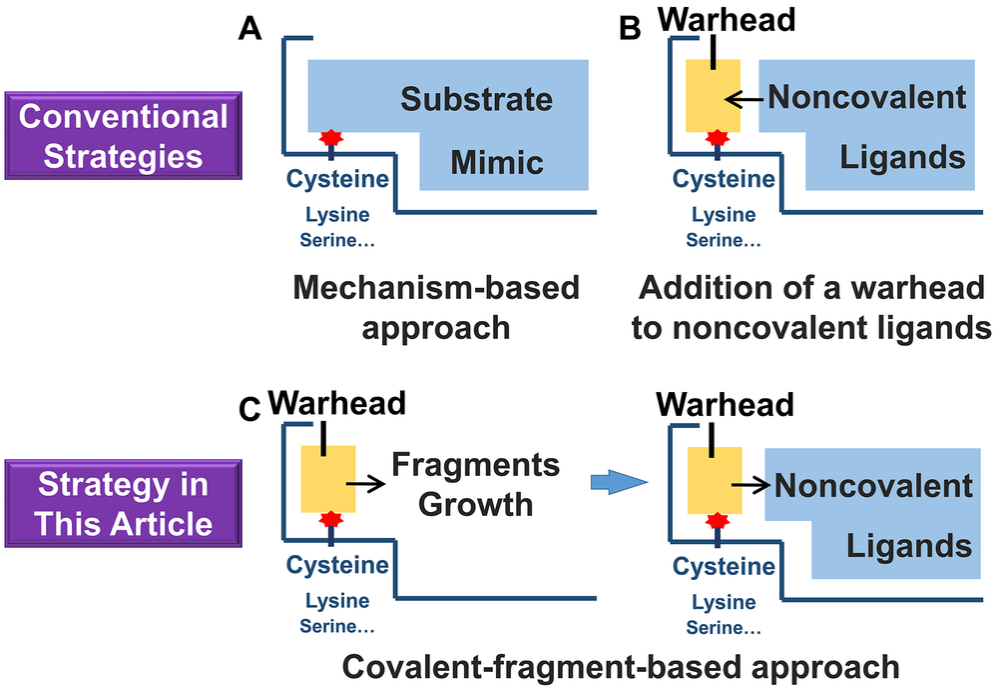

Figure 1. The strategies of covalent ligand design.

84x59mm (300 x 300 DPI)

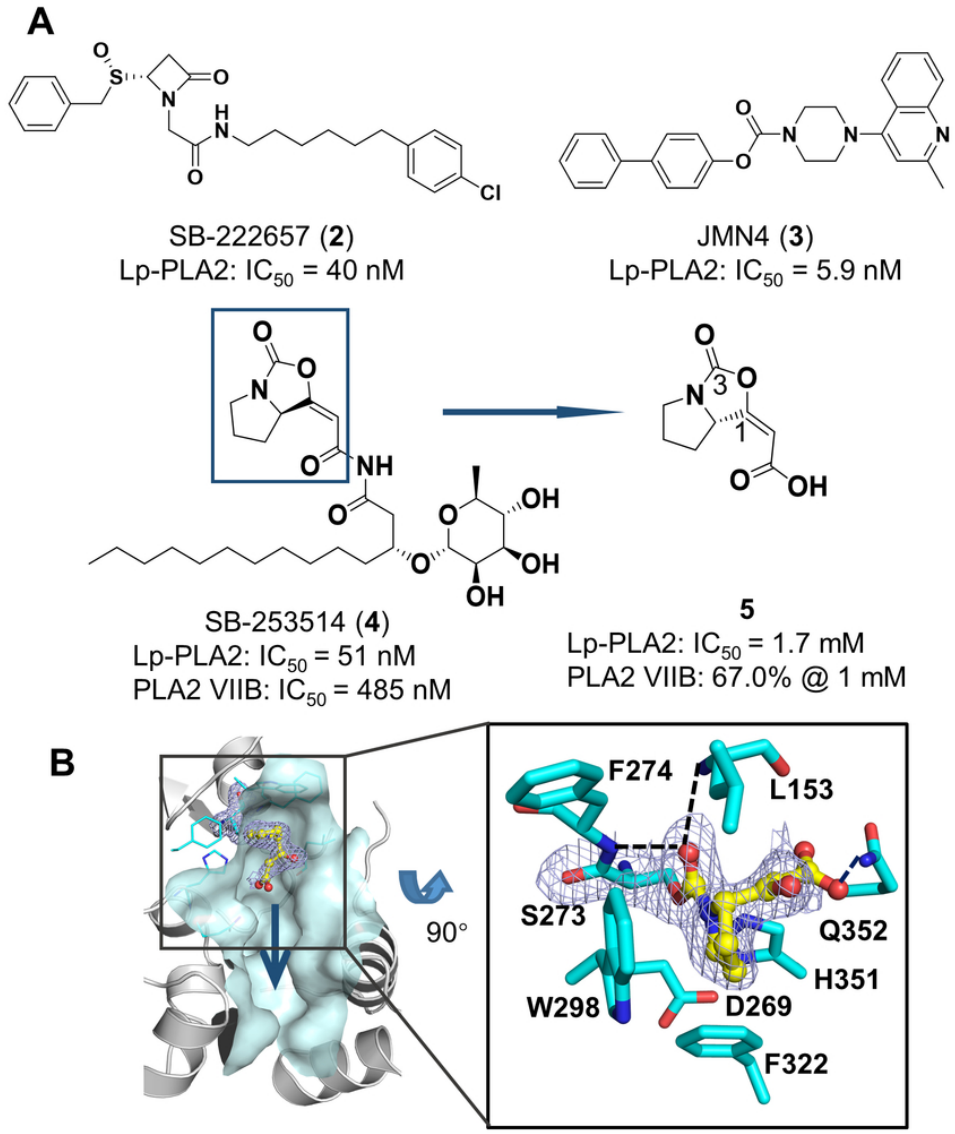

Figure 2. Covalent binding of the enol-cyclocarbamates to Lp-PLA2. (A) Structures of three suspected covalent inhibitors of Lp-PLA2 and fragment 5. The inhibition of fragment 5 against Lp-PLA2 and PLA2VIIB was shown under the structure. (B) A co-crystal structure of fragment 5 covalently bound to Lp-PLA2 (PDB code: 6M06). The direction for fragment 5 to grow into a more potent ligand is shown by a blue arrow. A close-up view of the binding pocket, in which fragment 5 (yellow) together with surrounding residues (cyan) are shown as sticks and H-bonds are represented by dashed lines. The mesh depicts the (2Fo-Fc) difference electron-density maps of the fragment contoured at 1.2 σ.

74x86mm (300 x 300 DPI)

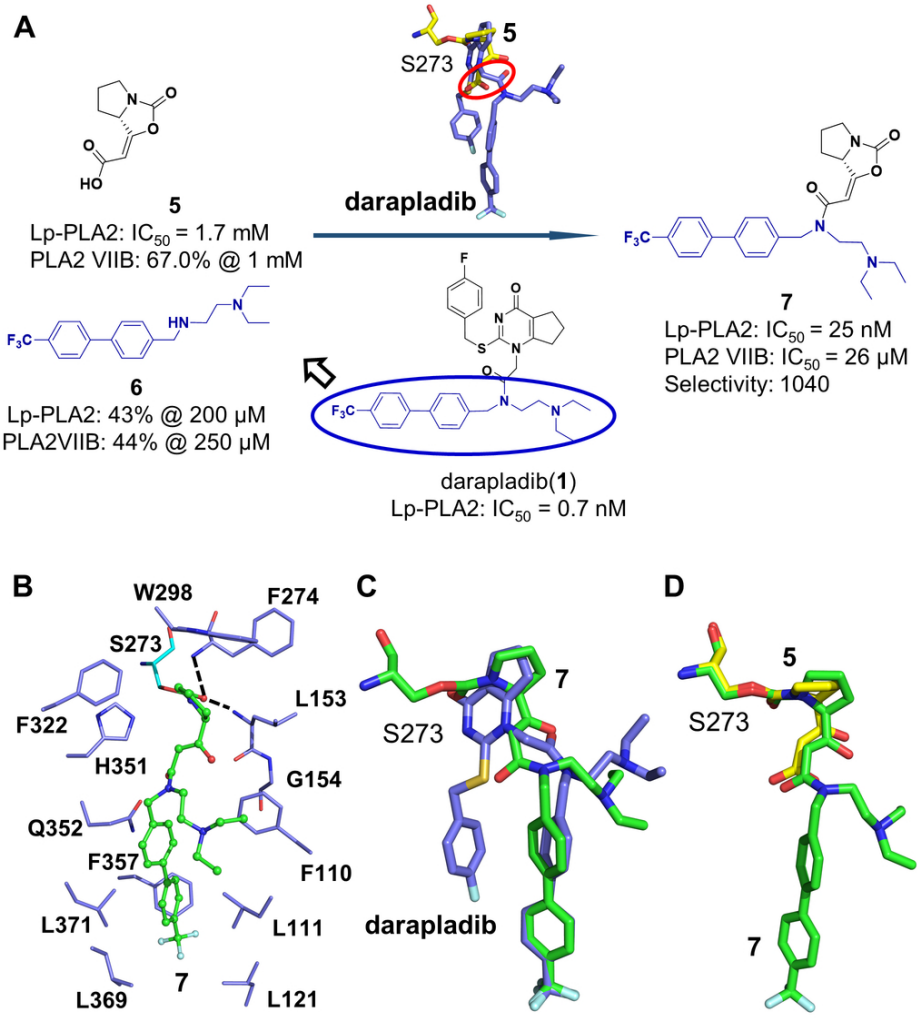

Figure 3. The discovery of compound 7 by a fusion of the covalent enol-cyclocarbamate and darapladib. (A) Schematic description for the design of compound 7 based on fragment 5 and darapladib. A red circle indicates the proximity between the amide of darapladib and the carboxyl of 5 by superimposing the co-crystal structures of Lp-PLA2 in complex with 5 (yellow) and darapladib (blue). (B) The Lp-PLA2-7 complex structure reveals interactions of 7 (green) with residues (blue) in the substrate binding pocket (PDB code: 6M08). H-bonds are represented by dashed lines. (C, D) Structure superimposition of Lp-PLA2-7 on Lp-PLA2-darapladib (C) or Lp-PLA2-5 (D).

93x96mm (300 x 300 DPI)

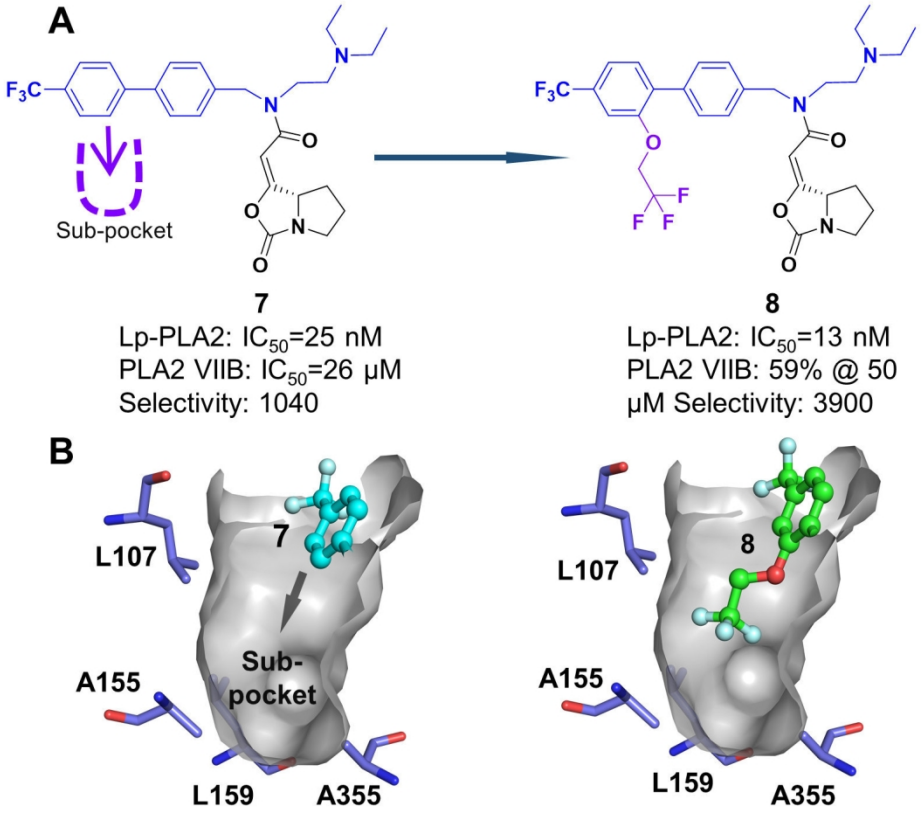

Figure 4. The discovery of compound 8 with high potency as well as selectivity for Lp-PLA2 over PLA2VIIB. (A) Schematic description for structure-based optimization of compound 7 to yield compound 8. (B) The co-crystal structures of Lp-PLA2-7 and Lp-PLA2-8 (PDB code: 6M07) complexes, in which a sub-pocket marked with a gray arrow was perfectly occupied by the introduced trifluoro-ethoxyl group.

76x65mm (567 x 567 DPI)

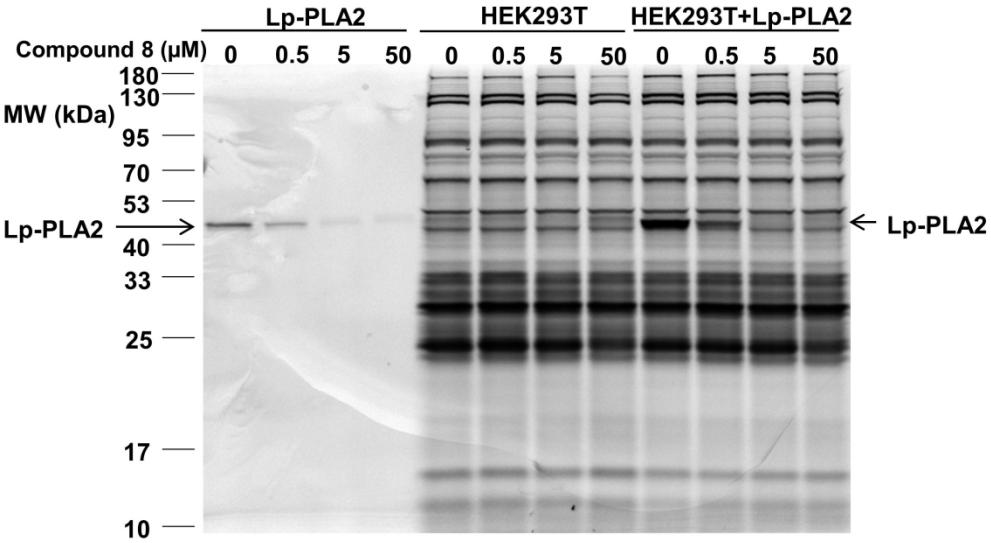

Figure 5. Selectivity evaluation of compound 8 in cells by the gel-based competitive ABPP probed with FP-TAMRA which is a non-selective covalent fluorescent probe of serine hydrolases. By comparison, the recombined human Lp-PLA2, the HEK293T lysate and the mixture of these two were used in the first, second and third four samples, respectively, and an in-gel fluorescence scanning was performed on all the samples.

171x94mm (410 x 410 DPI)

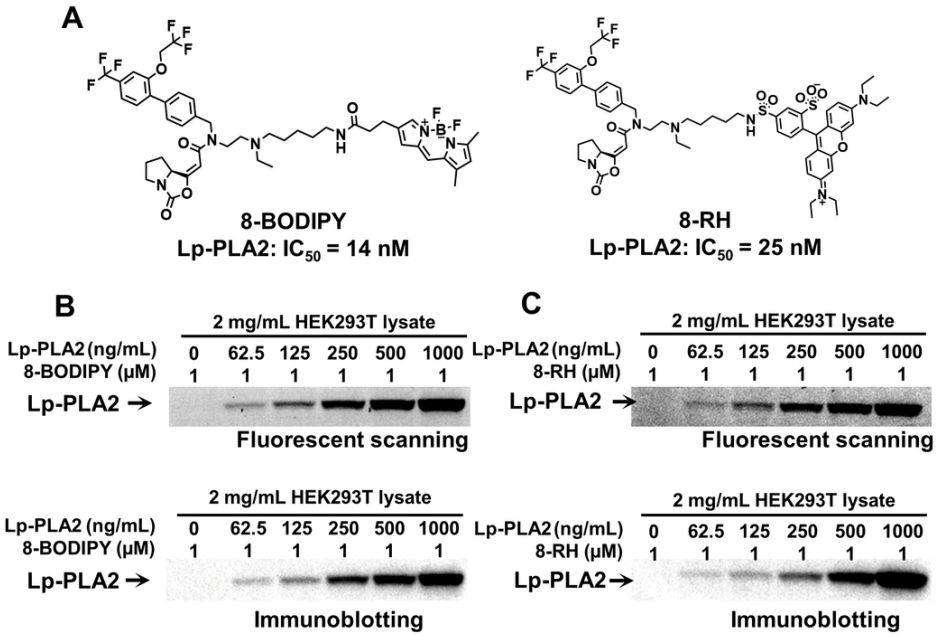

Figure 6. (A) Chemical structures of 8-BODIPY and 8-RH. (B, C) An in-gel fluorescence scanning using 8-BODIPY (B) or 8-RH (C) as a fluorescent probe with the HEK293T lysate added with different concentrations of recombinant human Lp-PLA2. An immunoblotting test was performed on the same gel used for the fluorescence scanning.

93x65mm (300 x 300 DPI)